

# POLITECNICO DI TORINO

Corso di Laurea Magistrale in Ingegneria Civile



Tesi di Laurea Magistrale

## **DEM studies of anticline - Boundary Conditions**

### **Relatori:**

Prof. Claudio Scavia

Prof. Gioacchino Viggiani

Prof. Juan Carlos Santamarina

### **Candidato:**

Marco Gioiello

Marzo 2018

## ABSTRACT

---

An analysis of previously published research that investigated fracture evolution in anticline formation highlighted several methodological limitations. These research uses the Discrete Element Method (DEM) to overcome these limitations. This research uses the DEM and large particles to simulate rock mass and to logically overcome scale related limitations of previous studies. The particles considered are a quantified unit of matter, a rock block, with scale-depending size. The Flat-Joint Model is used to define the bonded contact. A trial-and-error procedure matches the model micro-parameters with the physically reliable macro-properties of the two limestone rocks used in the simulations. Analysis of previous published literature derives the limestone macroproperties. The pre-modelling analysis is performed to avoid mechanical instability and to determine which aspects of geological features are essential to layer-parallel shortening models. These analyses allow us to model the initial shape of a pre-buckled anticline with a certain degree of confidence regarding the buckling physical and mechanical reliability. The layer-parallel shortening simulations used the pre-modelling analysis results. Investigations of the influence of extended domain uses single layer models. In addition, fracture evolution in multi-layered systems are also examined in layer-parallel shortening mechanism. A comparison of previous results with bending simulations enables the analysis of the influence of the loading process on fracture formations. The influence of the loading process on fracture evolution is investigated by comparing previous results with bending simulations. Bending simulations are performed for single and multi-layer models through rigid wall rotation. The influence of applied boundary conditions on the fracture evolution is analyzed for each model.

# Contents

---

1	Introduction.....	1
2	Anticline formation - Previous studies .....	3
2.1	Anticline .....	3
2.1.1	Anticline Formation .....	3
2.1.2	Folding mechanisms .....	4
2.1.3	Brittle rock failure in folding process .....	7
2.2	Previous Studies .....	9
2.2.1	Initial Fracture Influence.....	9
2.2.2	Mechanical-influencing parameters .....	10
2.2.3	Deformation-sensitive parameters .....	11
3	Method.....	13
3.1	Introduction to Discrete Element Method .....	13
3.2	Advantages of DEM.....	14
3.3	DEM for rocks.....	16
3.4	Flat-Joint Model (FJM) .....	18
3.5	Smooth-Joint Model (SJM).....	20
4	DEM calibration of rock .....	21
4.1	Macro-scale properties from literature .....	21
4.2	Calibration of micro-scale model parameters .....	23
4.2.1	Micro-scale parameters and their influence .....	23
4.2.2	Test procedures .....	24
4.2.3	Calibration procedures .....	25
4.3	Calibration results.....	26
4.4	Introduction to rock mass modeling (Synthetic Rock Mass) .....	28

5	Boundary conditions in anticline studies .....	29
5.1	Pre-modelling Analysis .....	29
5.2	Layer-parallel shortening .....	31
5.2.1	Models.....	32
5.2.2	Results.....	32
5.3	Bending .....	41
5.3.1	Models.....	41
5.3.2	Results.....	41
6	Conclusions.....	47
	Appendix – Rocks experimental data .....	49
	References.....	50

## LIST OF FIGURES

---

Figure 1.1: Anticline Trap.....	1
Figure 2.1 Fault-Related Folding: (a) Fault-bend folding; (b.1) Parallel fault-propagation folding; (b.2) Trishear fault-propagation folding; (c) Detachment folding. ....	4
Figure 2.2: Buckling – Loading schema on the left and a tectonic-scale example. 5	5
Figure 2.3: Bending - Loading schema (on the left), differential compaction (in the middle), and intrusion folding (on the right).....	5
Figure 2.4: Representation of failure related mechanics on Mohr diagram.....	7
Figure 2.5: (a) Fractures associated with folds; (b) Stress distribution in a bar of gelatin undergoing buckling by layer- parallel compression. The shaded area shows where the layer-parallel principal stress component is tensile (Twiss and Moores 1992). ....	8
Figure 2.6: Relationship between bed thickness and fracture spacing measured in sandy layers in wakes (data sets A, B and C) and Limestones (data sets D and E), (Twiss and Moores 1992).....	12
Figure 2.7: Stress versus Strain curves for extension experiments in weakly foliated Yule marble for constant strain rates at 500 C.....	12
Figure 2.8: Compression stress-strain curves of Soinhofen limestone at various temperatures at 40 MPa confining pressure. ....	12
Figure 2.9: Ductilities of water saturated rocks as a function of depth. Effects of confining (overburden) pressure, temperature and normal formation (pore) pressure are included (Stearns and Friedman 1972) .....	12
Figure 3.1: Models: (a) Bounded Contact Model (BCM), (Cundall and Strack 1979); (b) Bounded Particle Model (BPM),(Potyondy 2004); (c) Flat-Joint Model (FJM), (Potyondy 2013). ....	17
Figure 3.2: Three Flat-Joint contact types after (Wu and Xu 2016). ....	18
Figure 3.3: Strength envelopes of bonded and unbonded elements, (Wu and Xu 2016). ....	19
Figure 3.4: Smooth joint contact model between ball 1 and ball 2. Surface 1 and surface 2 denote either side of the joint lying at a dip angle of $\theta_p$ , after (Itasca 2011). ....	20

Figure 4.1: Hoek-Brown envelope of eight different Limestones. Data elaborated from (Tsiambaos and Sabatakakis 2004). .....	22
Figure 4.2: Specimens for (a) Unconfined Compressive test, (b) direct tension test and (c) Biaxial test. ....	25
Figure 4.3: Trial-and-error calibration procedure flow-chart, modified after (Chen). .....	26
Figure 4.4: Results of tests for the calibration of Rock Type 1. ....	27
Figure 4.5: Results of tests for the calibration of Rock Type 2. ....	27
Figure 5.1: Dimensionless plot of layer-parallel behavior. ....	30
Figure 5.2: Burial depth related mechanism depending on thickness ratio between burial depth and layer thickness ( $H/h$ ). ....	31
Figure 5.3: Layer-parallel shortening: (a) Affected domain single layer model; (b) Extended domain single layer model; (c) Multi-layer model; (d) Table of used rocks. ....	34
Figure 5.4: Layer-parallel shortening results of affected domain single layer model - Global axial stress-strain curve and number of partial cracks evolution. ....	35
Figure 5.5: Layer-parallel results for affected domain single layer model - fracture state on the top and force chain on the bottom, of each pair, for steps (1), (2) and (3) defined in “Figure 5.4”. ....	36
Figure 5.6: Layer-parallel shortening results of extended domain single layer model - Global axial stress-strain curve and number of partial cracks evolution. ....	37
Figure 5.7: Layer-parallel results for extended domain single layer model - fracture state on the top and force chain (where blue indicates compression and green tension) on the bottom, of each pair, for steps (1), (2) and (3) defined in “Figure 5.6”. ....	38
Figure 5.8: Layer-parallel shortening results of extended domain multi-layer model - Global axial stress-strain curve and number of partial cracks evolution. ....	39
Figure 5.9: Layer-parallel results for extended domain multi-layer model - fracture state on the top and force chain (where blue indicates compression and green tension) on the bottom, of each pair, for steps (1), (2) and (3) defined in “Figure 5.8”. ....	40

Figure 5.10: Bending: (a) Single-layer model; (b) Multi-layer model; (c) Table of used rocks.....	43
Figure 5.11: Bending results of single layer model - Global axial stress-strain curve and number of partial cracks evolution.....	44
Figure 5.12: Bending single layer model - fracture state on the top and force chain (where blue indicates compression and green tension) on the bottom of each pair, for steps (1), (2), (3), (4) and (5) defined in “Figure 5.11”.....	44
Figure 5.13: Bending results of multi-layer model - Global axial stress-strain curve and number of partial cracks evolution.....	45
Figure 5.14: Bending multi-layer model - fracture state on the top and force chain (where blue indicates compression and green tension) on the bottom of each pair, for steps (1), (2), (3), (4) and (5) defined in “Figure 5.13”.....	45
Figure 5.15: Bending multi-layer model – Displacement field and crack sequence for steps (1), (2), (3), (4) and (5) defined in “Figure 5.13”.....	46

## LIST OF TABLES

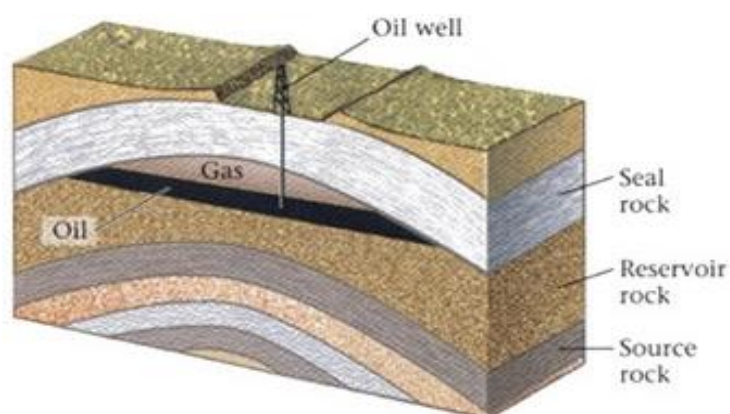
---

Table 4.1: Standard Deviation (STD) and tensile strength ( $\sigma_t$ ) evaluated from Hoek-Brown envelope and values of cohesion (c) and friction angle ( $\phi$ ) from analysis of data.....	22
Table 4.2: Influence of micro parameters on macro properties. ....	24
Table 4.3:Micro-scale parameters of characterized rock types.....	25

# 1 INTRODUCTION

---

Anticlines, structural domes, fault zones and stratigraphic traps are very favorable locations for oil and natural gas production. Represent the most commonly sought after and prolific traps. The accumulation is controlled dominantly by the top seal capacity versus the structural closure relief (*Dolson 2016*). Essentially a trap is an underground rock formation that blocks the movement of petroleum and causes it to accumulate in a reservoir which can then be exploited. The trapped oil is accompanied by water and often by natural gas; all are confined in a porous and permeable reservoir rock, which is usually composed of sedimentary rock such as limestones, sandstones and dolomites. A layer of impermeable rock, called the cap rock, prevents the upward or lateral escape of the petroleum. That part of the trap actually occupied by the oil and gas is called the petroleum reservoir.



*Figure 1.1: Anticline Trap.*

Anticline traps hold about 80 percent of the world's known oil reserves (*McLeish 1992*). A significant example is the Ghawar Field, by far the largest conventional oil field in the world and accounts for more than half of the cumulative oil production of Saudi Arabia (*Staff 1959*). This oil field is an anticline approximately 225-km long and 25-km wide in the subsurface (*Saner et al. 2005*). The estimated current production in the Ghawar Field, 5'000'000 barrels of oil and 57'000'000 m<sup>3</sup> of gas per day, shows the economic relevance of anticline traps. Furthermore, the presence of limestone in the Saudi field represents another common feature with many other reservoirs in the world such as in Mexico, Canada and Texas (*Howard 1928; Muir 1934; Staff 1959*). Most rocks possess fractures and other discontinuities which facilitate storage and fluid flow. On the other hand, some

discontinuities such as faults and dikes may also act as barriers to flow. Main flow paths in fractured rocks are along joints, fractures, shear zones, faults and other discontinuities. A common situation for fracture corridors to occur is within large, anticlinal traps where a thick stratigraphic succession is strongly layered (*Questiaux et al. 2010*). It is not clear when fracture corridors occur because of a single causative event. In other words, there may be several distinct tectonic processes that lead to the development of such corridors in different traps (*Questiaux et al. 2010*). Understand the formation mechanism and fracture-fluid interaction is important for several reasons in the oil industry. First, production from naturally fractured reservoirs with low matrix permeability, such as chalk or gas-bearing shale, is often only possible because a connected fracture system exists that can deliver the hydrocarbons to the producing well (*Lavrov 2016*). Fractures can also have a negative influence, such as leaks due to fracture related pathways in seal layer. Furthermore, the presence of fracture influence wellbores design and stability. Fractures create escape paths for drilling fluid and thereby constitute an important mechanism of lost circulation (*Lavrov 2016*).

The aim of this paper is to investigate the influence of different boundary conditions in the anticline formation models and fracture process with discrete element method. The art of modeling lies in determining what aspects of the geology are essential for the model (*Starfield and Cundall 1988*). Therefore simulation outcomes are imperfect but they can provide important insights. Judgment is invariably an essential aspect of this work. Simulationists try to maximize fidelity to theory, to mathematical rigor, to physical intuition, and to known empirical results. But it is the simultaneous confluence of these efforts, rather than the establishment of each one separately, that ultimately gives us confidence in the results (*Winsberg 2010*). Basing on preliminary studies the reliability of simple anticline mechanism models is evaluated.

## 2 ANTICLINE FORMATION - PREVIOUS STUDIES

---

### 2.1 ANTICLINE

Anticlines are folds in which the older layers are on the concave side of a bedding surface, and the younger layers are on the convex side. Thus these terms are only used if the relative ages of the folded layers are known. If they are not known, then we describe a convex-up fold as an antiform and a concave-up fold as a synform. Most anticlines are convex up (antiformal), although this geometry is not universal. In areas of complex deformation where the entire stratigraphy has been overturned, anticlines actually may be synformal (*Twiss and Moores 1992*). A geological fold occurs when one or a stack of originally flat and planar surfaces, such as sedimentary strata, are bent or curved as a result of permanent deformation.

#### 2.1.1 Anticline Formation

Folds in rocks vary in size from microscopic scale to mountain-sized folds in orogenic belts. Folds are commonly formed by shortening of existing layers (*layer-parallel shortening*), but may also be formed as a result of displacement on a non-planar fault (*fault bend fold*), at the tip of a propagating fault (*fault propagation fold*) or intrusions tends to deform the surrounding country rock (*Ramsay and Huber 1987*). **The Layer-parallel shortening** takes place when a sequence of layered rocks is shortened parallel to its layering, this deformation may be accommodated in a number of ways, homogeneous shortening, reverse faulting or folding. This represents the most common cause and is associated with mechanical instability also is known as buckling. The response depends on the thickness of the mechanical layering and the contrast in properties between the layers. If the layering does begin to fold, the fold style is also dependent on these properties (*Ramsay and Huber 1987*).

Many folds are directly related to faults, associate with their propagation, displacement and the accommodation of strains between neighboring faults. Some examples of **Fault-related folding** are *Fault bend folding*, *Fault propagation folding* reported in Figure 2.1. *Fault-bend folds*, showed in Figure 2.1 (a), occur where a thrust fault steps up from a structurally lower flat to a higher flat. This

anticline terminates downward into the upper flat. Fault bend folds occur in both extensional and thrust faulting (Suppe 1983). Fault-propagation folding, occurs when a propagating thrust fault loses slip and terminates up-section by transferring its shortening to a fold developing at its tip. Because of the variation in mechanical properties of layered sedimentary units, this mechanism may operate only within some units of a multi-layered sequence (Mitra 1990). The two main type of propagation, Parallel Fault-propagation Folding and Trishear Fault-propagation Folding, are represented in Figure 2.1(b).

**Detachment folds** form in sedimentary units with significant thickness and competency contrasts due to tectonics movements as shown in Figure 2.1(c). The basal layer is usually an incompetent unit, such as shale or salt, and is overlain by thick competent units such as carbonates or sandstones. The fold geometry and evolution are strongly dependent on the mechanical stratigraphy, including the thickness, ductility, and stratigraphic sequence of the units. In the early stages of fold tightening, the upper competent units are deformed primarily by hinge migration without appreciable internal deformation. Continued deformation results in a progressive reduction of the synclinal area through hinge migration. Variations in the geometry of detachment fold geometry, are related to variations in the initial mechanical stratigraphy and pre-existing structure (Mitra 2003).

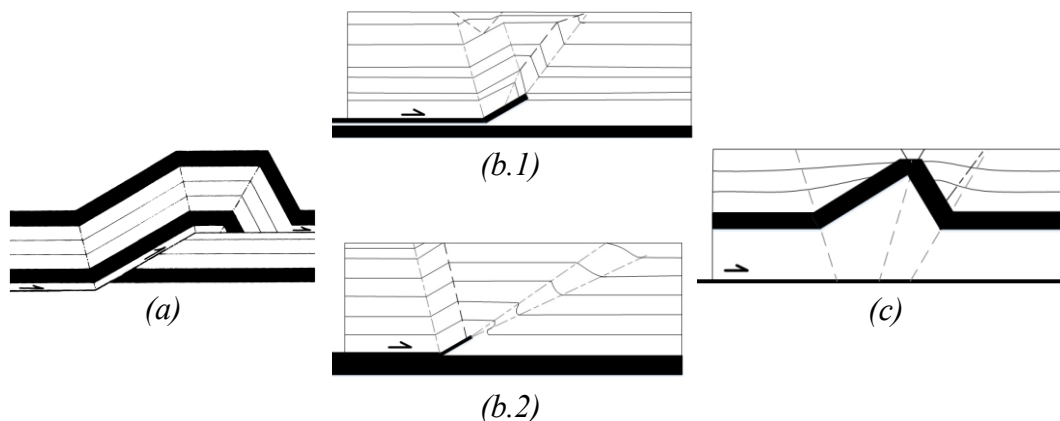


Figure 2.1 Fault-Related Folding: (a) Fault-bend folding; (b.1) Parallel fault-propagation folding; (b.2) Trishear fault-propagation folding; (c) Detachment folding.

## 2.1.2 Folding mechanisms

There is no unified classification of folding formation mechanism, due to different approaches and the strong dependence on boundary conditions. Many

classifications can be found in literature, based on different approaches (*Ramsay and Huber 1987*). From a geomechanical point of view, the main folding mechanisms based on stress condition applied on a layered rock, highlighting the multilayer fold controlling factors.

**Buckling** results from the application of compressive stresses parallel to a competent layer. If the compressive stress is sufficiently large, the layer becomes unstable and buckles into a fold (Figure 2.2) either under compressive stresses alone or in association with additional torques (*Ramsay and Huber 1987; Twiss and Moores 1992*). The presence of layers with contrasting competence produces a mechanical anisotropy, which is essential for buckling. The strong layer(s) fold(s) while the weaker matrix fills in gaps (*Burg 2017*).

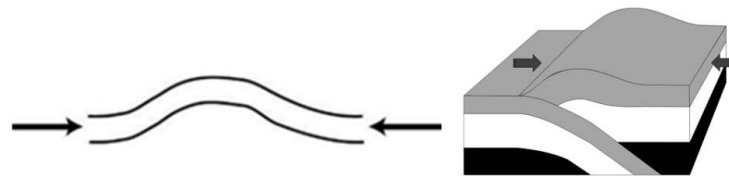


Figure 2.2: Buckling – Loading schema on the left and a tectonic-scale example.

**Bending** is a boundary condition or external load related model (*Ragan 2009; Ramsay and Huber 1987*). These boundary conditions or external load originate at different scale occur (Figure 2.3) such as in a *Lithospheric-scale*, in subduction zones and in cratons where vertical stresses produce broad domes, basins, swells and arches of originally horizontal bedding. Downscaling, *Crustal-scale bending* produces gentle up/down-warping and some examples are intruding pluton, drape folds and forced folds, while in the *Mesoscale bending* folds can occur on outcrop scale around local objects (*Burg 2017*).

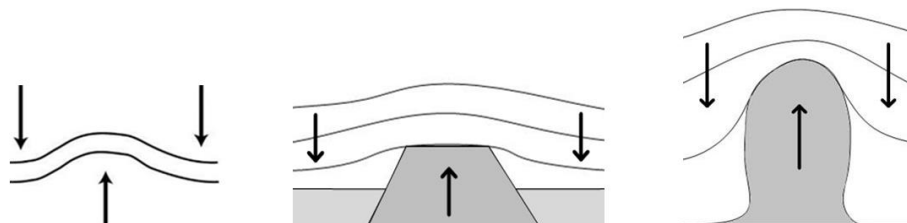


Figure 2.3: Bending - Loading schema (on the left), differential compaction (in the middle), and intrusion folding (on the right).

**Passive shear folding** is produced by simple shear, it can be formed in response to any kind of ductile strain. Passive folding produces harmonic folds where the

layering plays no mechanical role and therefore no influence on the fold shape (Ragan 2009). A deck of cards is a good example to illustrate the shear folding process, as a layer was drawn on the sides of the deck. When one card differentially move relative to another, they produce a fold by a mechanism called Shear Folding (Twiss and Moores 1992). The wide range of fold style and size arises because of the mechanical instabilities in a *multilayered* sequence depending upon a number of *factors that controls the fold geometry* which are:

1. The *composition of layers* and the primary *rheological properties* of each rock type.
2. Changing the *pressure and temperature* conditions as a reason for changing in rheological properties of the layers during the period of fold formation.
3. The development of *orientation of mineral grains* during deformation as a result of mechanical rotation or recrystallization processes.
4. The *thickness* of each stock layer in rock packet, and if the different rock layers are grouped into units.
5. The *scale of folding* is an important factor which decides whether or not gravitational force exerts an influence on the fold geometry.
6. The nature of *boundary constraints* on the rock units undergoing folding.
7. The *mechanical properties of the interfaces between layers* which control strongly the development of a fold.

(Ramsay and Huber 1987)

Furthermore, these factors have a strong influence also on the strain pattern, as shown in 2.2 - Previous Studies, due to the strong influence on mechanisms such as **Flexural slip/Flow folding**. Where layering exerts a strong influence in the folding of a rock sequence, flexing of layers is accomplished by slipping of one layer past another, by flow within the layers, or by a combination of the two. In each case, the layering controls the mechanism of folding and, hence, the geometry and internal features of the resultant fold. The cohesion between layers is commonly less than that within layers, and slip occurs if the shear stress on the surface of the layers exceeds the cohesion and frictional resistance to slip between these layers (Donath and Parker 1964). Any bending of layers causes stresses to develop resisting that strain, where for thick layers plastic strains are large. Consequently, if layer parallel

slip is possible, some interfaces can slip with smaller strain requirements. Work associated with strain, and work related to slip, are minimized. An example is Rattlesnake Mountain, where flex slip allows strains to be accomplished by fracturing (Couples et al. 1998).

### 2.1.3 Brittle rock failure in folding process

The state of current knowledge of the brittle mechanical properties of rock, as determined in laboratory experiments on relatively small specimens of intact rock, is long reported in literatures (Paterson and Wong 2005). The distinction between brittle and ductile behavior is a macroscopic one, depending on whether or not the rock specimen is capable of undergoing substantial permanent strain without macroscopic fracture, which is described as “brittle fracture” when it is not preceded by any appreciable amount of permanent deformation. The two principal modes of brittle failure are presented in Figure 2.4. *Shear fracture*, in which the relative displacement is parallel to the fracture surface, and *extension fracture*, in which the relative displacement is normal to the fracture surface (Burg 2017; Stearns and Friedman 1972).

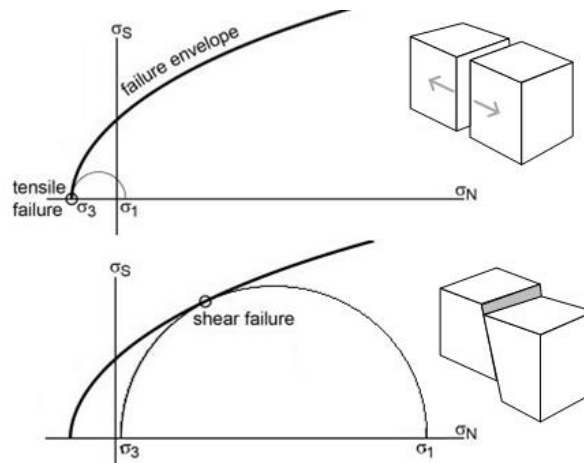
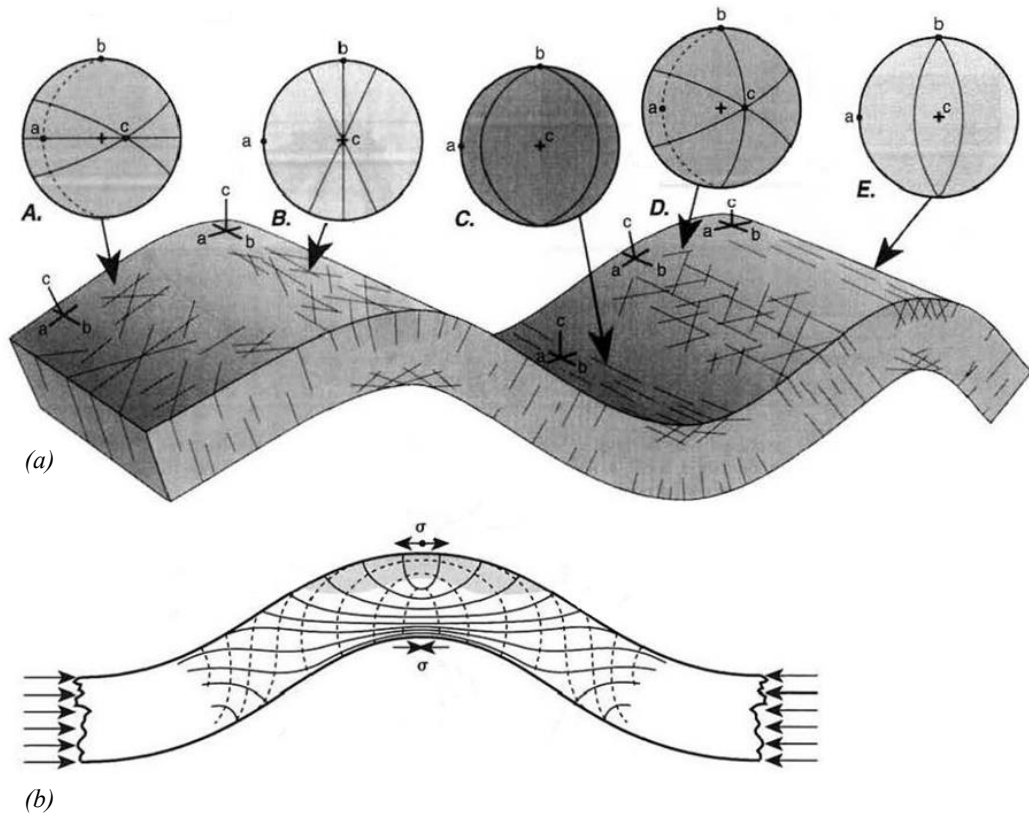


Figure 2.4: Representation of failure related mechanics on Mohr diagram.

Furthermore, though not restricted to the brittle domain, rupture is everywhere involved in the deformation of rocks. It follows that those parameters that tend to increase rock ductility also tend to decrease the dependency on rupture. Extensive laboratory studies of the mechanical properties of common sedimentary rocks have been published and the main results are reported in Section 2.2 - Previous Studies.

Fractures geometrically related to folds may originate during folding. In that case, they may reflect some elongation of rocks, often parallel to fold hinge lines. If produced after folding, they have orientation influenced by the mechanical anisotropy of folded rock (Burg 2017). Under several assumptions such as the elastic behavior of layers (treated as an elastic beam), neglecting the geological history load, etc., a theoretical fracture network is proposed by *Twiss and Moores (year)*. The influence of these assumptions will be analyzed in Section 2.2 - *Previous Studies*. According to the mechanics of fractures presented before (*Figure 2.4*) and the Stress trajectories (*Figure 2.5b*), after folding fractures network is obtained and presented in *Figure 2.5 (a)* (*Twiss and Moores 1992*).



*Figure 2.5: (a) Fractures associated with folds; (b) Stress distribution in a bar of gelatin undergoing buckling by layer- parallel compression. The shaded area shows where the layer-parallel principal stress component is tensile (Twiss and Moores 1992).*

## 2.2 PREVIOUS STUDIES

Natural fractures impact the performance of many reservoirs around the world, including some of the carbonate reservoirs in the Middle East (*Nelson 2001*). Knowledge of the controlling fracture in a given reservoir not only aids in the primary recovery of hydrocarbons but also guides in the design of secondary recovery programs (*Stearns and Friedman 1972*). A general review of fractured reservoirs and their economic significance was given by (*Drummond 1964; Hubbert and Willis 1955*). In the last decades, several studies have been made in order to identify the main factor that influences the fracture network in a folded system, and in general reservoir, with different methods. Fracture prediction is commonly based on geometric and/or kinematic models such as analyses of fold curvature (*Allwardt et al. 2007; Ericsson et al. 1998; Fischer and Wilkerson 2000; Hennings et al. 2000; Keating and Fischer 2008; Masaferrero et al. 2003*) or seismic-based techniques (*Masaferrero et al. 2003*) but far less commonly with geomechanical modelling (*Gross et al. 1995; Guo et al. 2017; Sanz et al. 2008; Smart et al. 2009*).

### 2.2.1 Initial Fracture Influence

Much of the research on structurally controlled fracture prediction has focused on the relationship between fold shape and strain accommodated within the folded layers. Several relationships have been proposed to predict fracture characteristics based on outcrop studies (*Corbett et al. 1987; Di Naccio et al. 2005; Ferrill et al. 2007*), laboratory experiments (*Bazalgette and Petit 2007; Galuppo et al. 2016; Rives et al. 1992*) and analyses of drilling and production data from existing fields. For example, a positive correlation between fracture intensity and layer curvature has been posted in some geologic structures (*Murray Jr 1968; Stewart and Podolski 1998*), although this relationship has been proven to not hold universally (*Hennings et al. 2000; Keating and Fischer 2008*). The underlying assumption in curvature-based analyses is that the layer curvature is a proxy for strain based on elastic plate-bending theory (*Ramsay 1967*). The main limitation of this approach lies in the reactivation of existing fractures (either shear or opening) instead of forming new fractures (*Bergbauer and Pollard 2004; Twiss and Moores 1992*) since

Folding/bending is not the only mechanism that may cause fracturing (*Twiss and Moores 1992*). Curvature analysis on the present day geometry does not consider geological history, and consequently the initial fracture controls, and might significantly underestimate the total deformation throughout geological time (*Ferrill et al. 2007; Gholipour 1998*). Recognized the strong influence of geological history on natural fracture network, the difference between mechanical stratigraphy and fracture stratigraphy needs to be clarified; (*Laubach et al. 2009*). Mechanical stratigraphy subdivides stratified rock into discrete mechanical units defined by properties such as tensile strength, elastic stiffness, brittleness, and fracture mechanics properties. Fracture stratigraphy subdivides rock into fracture units according to extent, intensity, or some other observed fracture attribute. Furthermore, the mechanical stratigraphy is the variation of rock properties through a lithostratigraphic column, but it is essential to appreciate that these rock properties also can vary with time (*Hayes and Hanks 2008*). Fracture stratigraphy reflects a specific loading history and mechanical stratigraphy during failure (*Hayes and Hanks 2008; Laubach et al. 2009*).

### **2.2.2 Mechanical-influencing parameters**

The influence of mechanical and geometric parameters on fracture stratigraphy have long been studied. Rupture are commonly recognized to be influenced by the composition, geometries and primary rheological properties of the layer as well as from temperature, effective confining pressure, and strain rate as reported in *Figure 2.6, Figure 2.8, Figure 2.8 and Figure 2.10* (*Ramsay and Huber 1987; Stearns and Friedman 1972*). Increasing effective confining pressure or temperature or decreasing strain rate tends to increase ductility (*Ramsay and Huber 1987*). Understanding and interpreting the fracture intensity, with timing and orientation, is commonly important in the fracture network prediction. Several studies have found that fracture spacing is positively correlated with layer thickness (*Ji et al. 1998; Narr and Suppe 1991; Rives et al. 1992*), whereas other workers suggest that mechanical stratigraphy maybe more important than simply layer thickness (*Cooke et al. 2006; Corbett et al. 1987; Wennberg et al. 2006*). Furthermore, (*Ji et al. 1998*) showed three categories of mechanical models to explain the relationship between mean joint spacing and bed thickness, highlighting the lack of a fundamental aspect

in many studies. Although each of the models mentioned above has contributed to progress in the mechanical analysis of joint spacing, an obvious problem is that they have ignored the effects of possible slip on bed interfaces. All the previous models assumed that bedding interfaces are perfectly bonded so that there is no slip between the layers (*Ji et al. 1998*). The presence or absence of interlayer slip is shown to control the distribution and evolution of strain strongly, and this control has important implications for interpreting fractures from geomechanical models (*Smart et al. 2009*).

### **2.2.3 Deformation-sensitive parameters**

Factors that determine the deformation style are identified. For instance, the impact of the layered anisotropic nature of sedimentary rocks and variations in competence, from layer to layer, are recognized as deformation style important factors (*Donath and Parker 1964; Ramsay 1967*). The aforementioned interlayer slip importance on fold evolution and final fold shape is also well known. Where layering exerts a strong influence in the folding of a rock sequence, flexing of layers is accomplished by slipping of one layer past another, by flow within the layers, or by a combination of the two. In each case, layering controls the mechanism of folding and, hence, the geometry and internal features of the resultant fold. The cohesion between layers is commonly less than that within layers, and slip occurs if the shear stress on the surface of the layers exceeds the cohesion and frictional resistance to slip between these layers (*Donath and Parker 1964*). Any bending of layers causes stresses to develop resisting that strain, where for thick layers the plastic strains are large. Consequently, if layer parallel slip is possible, some interfaces can slip with smaller strain requirements (*Couples et al. 1998; Erickson 1996*). Work associated with strain, and work related to slip, are minimized. An example is Rattlesnake Mountain, where flex slip allows strains to be accomplished by fracturing (*Couples et al. 1998*).

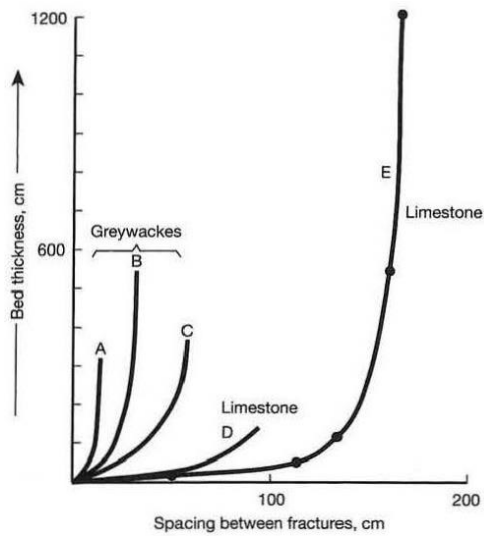


Figure 2.6: Relationship between bed thickness and fracture spacing measured in sandy layers in waxes (data sets A, B and C) and Limestones (data sets D and E). (Twiss and Moores 1992).

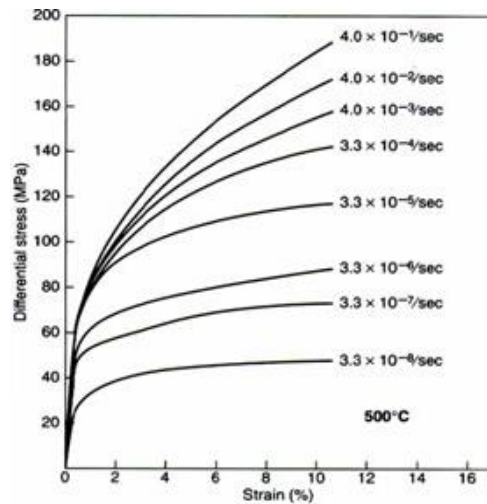


Figure 2.7: Stress versus Strain curves for extension experiments in weakly foliated Yule marble for constant strain rates at 500 C.

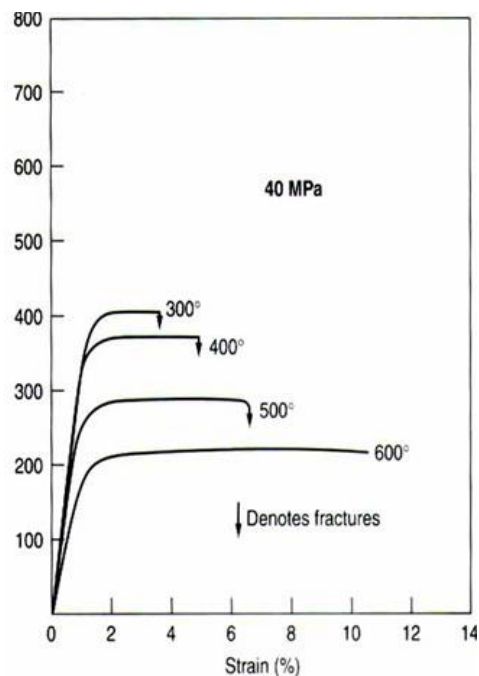


Figure 2.8: Compression stress-strain curves of Soinhofen limestone at various temperatures at 40 MPa confining pressure.

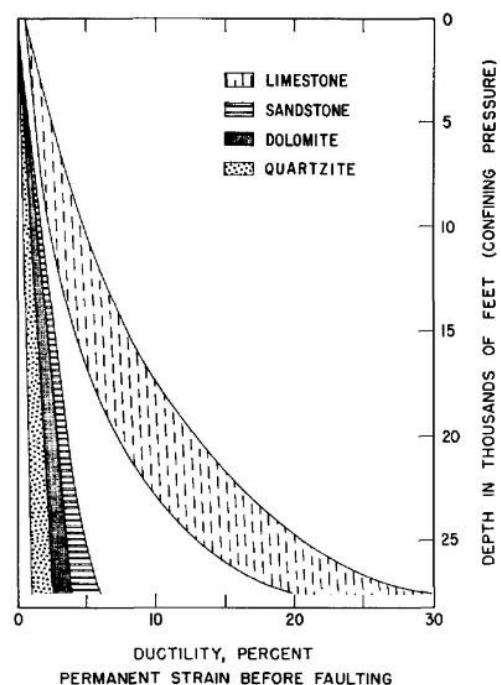


Figure 2.9: Ductilities of water saturated rocks as a function of depth. Effects of confining (overburden) pressure, temperature and normal formation (pore) pressure are included (Stearns and Friedman 1972)

## 3 METHOD

---

### 3.1 INTRODUCTION TO DISCRETE ELEMENT METHOD

Distinct Element Method (DEM) belongs to the simulation methods under the discontinuum assumption, and it models the motion of an assembly of bodies where the interaction between them is viewed as a transient problem with states of equilibrium evaluated for each time steps (*Cundall 1971; Cundall and Strack 1979; O'Sullivan 2011*). The distinct element method was introduced by (*Cundall 1971*) for the analysis of rock mechanics problems and then applied to soils by (*Cundall and Strack 1979*). Important to point out that the name “Discrete Element Method” is applied to a distinct element method based code only if it allows finite displacements and rotations of discrete bodies, including complete detachment, and recognizes new contacts automatically as the calculation progresses. Without the first attribute, the model cannot reproduce some important mechanisms in a discontinuous medium; without the second, the model is limited to small numbers of bodies for which the interactions are known in advance (*Cundall and Hart 1992*). DEM is based on the idea that the time step chosen may be so small that, during a single time step, disturbances cannot propagate from any particle further than its immediate neighbors. Then, at all times, the assembly of the bodies is obtained by calculations based on the discretized Newton’s second law, applied on the bodies, and a force-displacement law, applied on the contacts. While the discretized Newton’s second law gives the motion of a particle from the forces acting on it, the force-displacement law is used to find contact forces from displacements (*Cundall 1971; Cundall and Hart 1992; Cundall and Strack 1979*). There are three types of bodies: balls (or particles), clumps, and walls. Bodies have surface properties that are assigned to the pieces on the body surface. A ball consists of one piece, which is the ball itself, while the pieces of a clump and wall are called pebbles and facets, respectively. A ball is a rigid unit-thickness disk in 2D or sphere in 3D. A clump is a collection of pebbles that are rigid unit-thickness disks in 2D or spheres in 3D. The interaction behaviors of particles are simulated using three models: a stiffness model, a slip model, and a bond model. The stiffness model describes the elastic

behavior that relates the contact force and relative displacements in the normal and shear directions (*Wu and Xu 2016*). The slip model provides a friction coefficient, or residual friction angle, between particles, controlling the frictional strength of the particles. The bond model allows the particles to be cemented together. Based on the adopted solution algorithm we can define explicit and implicit methods. The term distinct element method refers to numerical codes that use an explicit time-domain integration scheme to solve the equations of motion for rigid or deformable discrete bodies with deformable contacts (*Cundall and Strack 1979*). The use of an explicit, as opposed to an implicit, numerical scheme, makes it possible to simulate the nonlinear interaction of a large number of particles without excessive memory requirements or the need for an iterative procedure. Current computing power limits the size of the atomic ensemble to numbers of atoms and molecules that are too small to be useful for most engineering-scale systems. Nevertheless, it may be possible to use the principle of the molecular dynamics method at the rock scale with a discrete element method. In doing so, the entity considered is no longer an atom but a quantified unit of matter, a rock block, the size of which depends on the scale of investigation (*Donzé et al. 1994*). For the purposes of studying the dominant fracture and failure behaviors of intact rock in the brittle regime, a representation at the grain scale should be sufficient, because the damage processes either occur at this scale or their effects can be mapped to this scale (*Potyondy 2015*).

## **3.2 ADVANTAGES OF DEM**

There are two primary motivations to use DEM in geomechanics. Firstly, in applied boundary value problems, discrete element methods can more easily simulate large-deformation problems than continuum-mechanics-based analysis tools. DEM simulations can also capture mechanisms such as arching or nucleation of cracks that are a consequence of the particulate nature of the material. The second use of DEM is as a tool in basic research. A discrete element simulation can probe the material response at a much more detailed scale than can be monitored even in highly sophisticated laboratory tests (*O'Sullivan 2011*). To paraphrase (*Weatherley 2009*), in a DEM simulation information which is “hidden” in conventional physical

experiments is revealed. Furthermore, for the aim of this paper and for rock material simulation in general, another motivation lies in the possibility to take into account pre-existing fracture and, conversely to continuum approach, the materials can fracture. This latter motivation makes this method a powerful tool for our purpose since, as mentioned in paragraph 2.2.1- Initial Fracture Influence. Previous Studies, the fracture pattern in a folded layer(s) is strongly influenced by the geological load history and the related fractures. Finite element, boundary element and Lagrangian finite difference programs have interface elements or “slide lines” that enable them to model a discontinuous material to some extent. However, their formulation usually is restricted in one or more of the following ways:

1. The logic may break down when many intersecting interfaces are used;
2. There may not be an automatic scheme for recognizing new contacts;
3. The formulation may be limited to small displacements and/or rotation

*(Itasca 2011; Lisjak and Grasselli 2014; O'Sullivan 2011).*

The software used in this paper is ***Particle Flow Code (PFC)*** in its two-dimension version (PFC2D). The PFC model is a distinct element modeling approach that encompasses both granular and solid materials, modeling the movement and interaction of stressed assemblies of rigid particles *(Itasca 2011)*. PFC is classified as a discrete element code based on the definition in the review by *(Cundall and Hart 1992)*, since it allows finite displacements and rotations of discrete bodies, and recognizes new contacts automatically as the calculation progresses. PFC can be viewed as a simplified implementation of the DEM because of the restriction to rigid (circular in 2D; spherical in 3D) particles. To notice that the term particle, as used here, differs from its more common definition in the field of mechanics, where it is taken as a body whose dimensions are negligible and therefore occupies only a single point in space. In the present context, the term particle denotes a body that occupies a finite amount of space. Thanks to its general design, PFC can be easily customized and applied to a very broad range of numerical investigations where the discrete nature of the systems is of interest *(Itasca 2011)*. The Python programming language is used to manipulate PFC models, used for the aim of this paper, in order to increase the power of PFC, e.g. using sophisticated broadcasting functions or using N-dimensional array object.

### 3.3 DEM FOR ROCKS

Rock behaves like a cemented granular material of complex-shaped grains in which both the grains and the cement are deformable and may break (*Itasca 2011; Potyondy 2012; Potyondy and Cundall 2004; Potyondy 2015*). Correspondences with this modeling are found in real rock since in sedimentary rock, such as sandstone, a true cement is present, whereas in crystalline rock, such as granite, the granular interlock can be approximated as a notional cement (*Potyondy and Cundall 2004*). The following behaviors are observed both in rock samples and in synthetic samples composed of bonded particles:

- continuously non-linear stress–strain response followed by softening or hardening;
  - Behavior that changes in character, according to stress state;
  - Memory of previous stress or strain excursions, in both magnitude and direction;
  - Dilatancy that depends on history, mean stress and initial state;
  - Hysteresis at all levels of cyclic loading/unloading;
  - Transition from brittle to ductile shear response as the mean stress is increased;
  - Dependence of incremental stiffness on mean stress and history;
  - Induced anisotropy of stiffness and strength with stress and strain path;
  - Non-linear envelope of strength;
  - Spontaneous appearance of microcracks and localized macrofractures;
- (*Potyondy and Cundall 2004*).

Given the correspondence of behaviors reported above the rock samples are studied as bonded particles. Three main models are presented in *Figure 3.1* as discussed in (*Wu and Xu 2016*): *Bounded Contact model (BCM)* with contact bonds, *Bounded Particle Model (BPM)* with parallel bonds and *Flat-Joint contact Model (FJM)* with flat-joint contacts which can be deformable, partially damaged and breakable (*Potyondy 2013; Wu and Xu 2016*). When the stresses acting on the bond exceed the corresponding strength, the bond will break. In this paper the Flat Join Model is used to simulate the bond between particles, it is shown in detail in the dedicated

section explaining the reason for this choice. The BCM, *Figure 3.1(a)*, is based on bonding point, thus can only consider force, while BPM, *Figure 3.1(b)*, uses a finite length bond, and thus it can undertake both force and moment. It should be noted that the slip model cannot exist simultaneously with the parallel bond model and only takes effect after the parallel bond broken. The parallel bond can be represented as two sets of springs, one parallel to the contacting surface between the two contacting particles and the other perpendicular to that surface. Each set of springs has its stiffness and strength parameters.

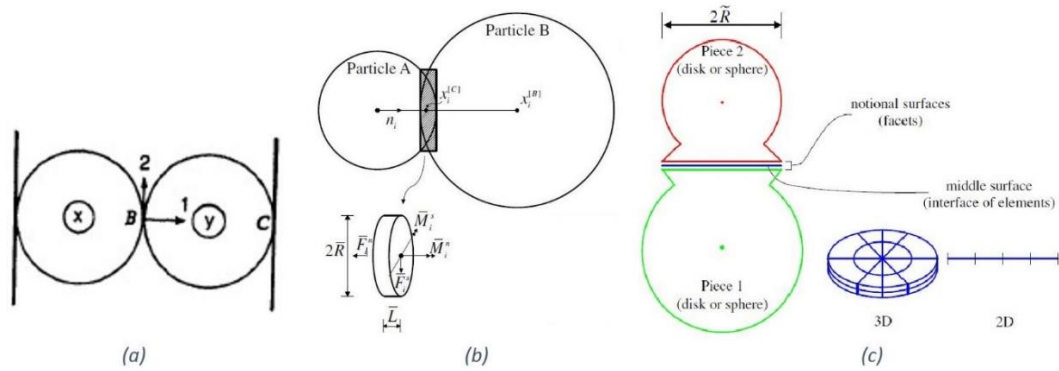


*Figure 3.1: Models: (a) Bounded Contact Model (BCM), (Cundall and Strack 1979); (b) Bounded Particle Model (BPM),(Potyondy 2004); (c) Flat-Joint Model (FJM), (Potyondy 2013).*

As mentioned before, one of the advantages of this method is that we can simulate the initial discontinuities in DEM model. Prior to performing a simulation, the interaction forces must be specified between all particles and their nearest neighbors. While an intact medium is specified by defining all initial interaction forces to be of the repulsive-attractive type with bounded contact, a pre-fractured medium can be specified by randomly or defined distribution of repulsive-only interaction forces among the particle pairs. The Smooth Joint Model (SJM) is also used in the codes and reported more in detail in the dedicated section below. This model simulates the behavior of an interface modifying the surfaces of the contacting grains to align with the interface and allows us to overcome the inherent roughness of interface surfaces in particle-based material discontinuities. This roughness typically results in an artificial additional strength along frictional or bonded rock joints (*Mas Ivars et al. 2008; Potyondy 2015*). The combination of bonded particle model, to capture the behavior of intact material, with the SJM for joint network leads to the development of the so-called synthetic rock mass

(Potyondy 2015), which aims at numerically predicting rock mass properties, including scale effects, anisotropy and brittleness, that cannot be obtained using empirical methods.

### 3.4 FLAT-JOINT MODEL (FJM)

The Flat-Joint contact Model, in *Figure 3.1(c)*, provides the macroscopic behavior of a finite-size, linear elastic, and either bonded or frictional interface that may sustain partial damage (Potyondy 2013). We refer to the balls of a flat jointed material as faced grains, each of which is depicted as a circular or spherical core and a number of skirted faces. The faced grains are created when the flat-joint contact model is installed at the ball–ball contacts of a packed ball assembly. The contact between two elements in FJM can be classified in three types and subdivided in two categories (Figure 3.2):

- Bounded elements: Type B (gap=0)
- Unbounded elements: Type G (Gapped contact, gap>0) and Type S (Slit contact, gap=0)

An interface exists between each set of adjoining faces and is discretized into elements (see *Figure 3.1(c)*) with each element being either bonded or unbonded.

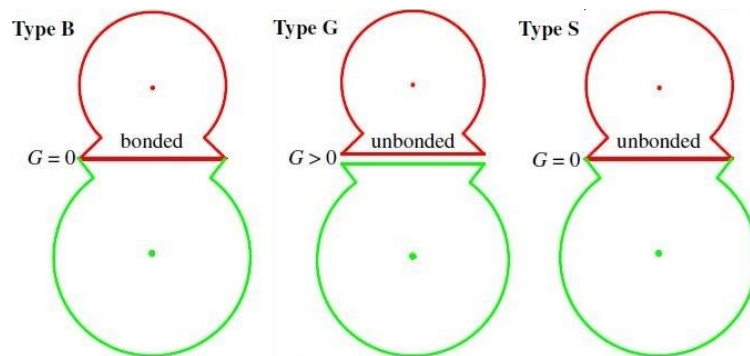


*Figure 3.2: Three Flat-Joint contact types after (Wu and Xu 2016).*

The breakage of each bonded element contributes partial damage to the interface, and each breakage event is denoted as a crack. The behavior of a bonded element is linear elastic until the strength limit is exceeded and the bond breaks making the element unbounded, while the behavior of an unbounded element is linear elastic and frictional with slip accommodated by imposing a Coulomb limit on the shear force, as showed in *Figure 3.3* below.

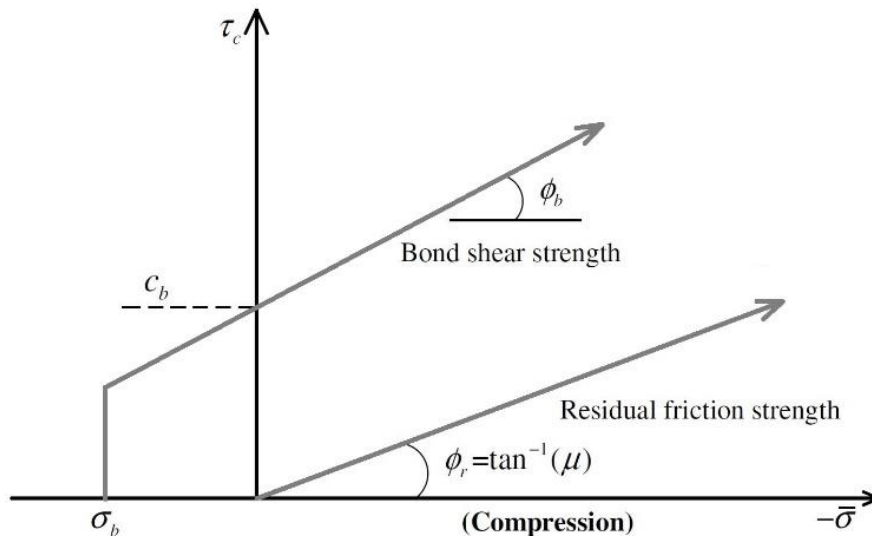


*Figure 3.3: Strength envelopes of bonded and unbounded elements, (Wu and Xu 2016).*

FJM is introduced since the BPM presents three main problems which are the unrealistically low UCS/TS ratio (brittleness), excessive low internal friction angle and the linear strength envelope which correspond a low  $m_i$  value in Hook-Brown's criteria. These problems arise for the spherical shape used in the models which provide an unreliable rotational resistance and grain interlocking. Other reasons for these problems are the no pressure dependence of the shear strength and unconsidered pre-existing crack. For these reasons the FJM is introduced, where the skirted particle shape can provide grain interlocking and rotational resistance even after the interface breaking. This last contact model increases the grain interlocking and provide proper rotational resistance due to its special structure.

### 3.5 SMOOTH-JOINT MODEL (SJM)

(Mas Ivars et al. 2008) extend the bounded particle model to include joints at a scale larger than the particles by creating a Smooth-Joint contact Model that allows each joint to be represented as a collection of smooth-joint contacts. The smooth-joint model simulates the behavior of a planar interface with dilation regardless of the local particle contact orientations along the interface.

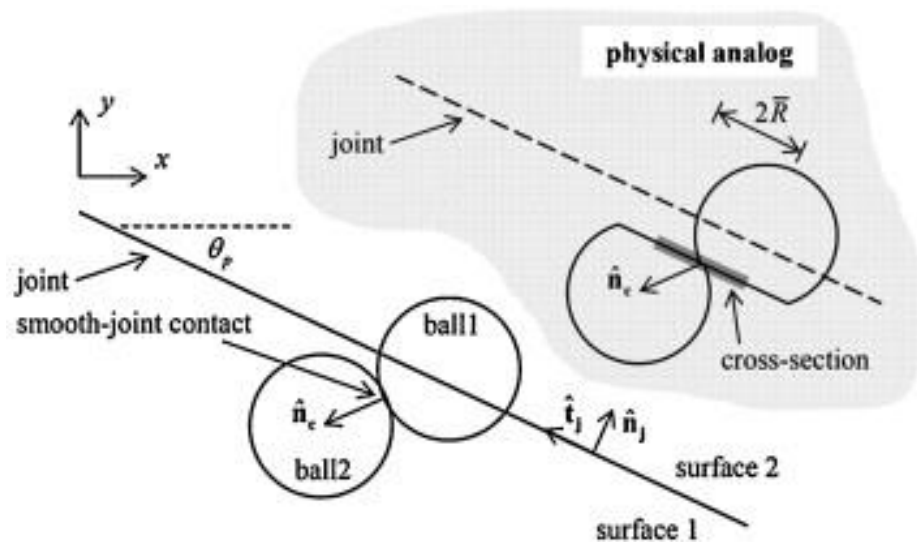


Figure 3.4: Smooth joint contact model between ball 1 and ball 2. Surface 1 and surface 2 denote either side of the joint lying at a dip angle of  $\theta_p$ , after (Itasca 2011).

The behavior of a frictional or bonded joint can be modeled by assigning smooth-joint models to all contacts between particles that lie on opposite sides of the joint as reported in Figure 3.4. The behavior of the bonded interface is linear elastic until the strength limit is exceeded and the bond breaks, making the interface unbounded; the behavior of an unbounded interface is linear elastic and frictional with dilation, with slip accommodated by imposing a Coulomb limit on the shear force, as showed in Figure 3.3 for FJM.

## 4 DEM CALIBRATION OF ROCK

---

In this chapter, the material characterization procedure is shown. We must empathize that the purpose is to reproduce a physical reliable behavior of rock and not to reproduce experimental results obtained on a rock. In order to do it, the proposed data collection and analysis methodology is reported below. Once inferred the range of reasonable macro-parameters of rock, two rock type has been characterized. The choose of these rock types is based on preliminary phenomena studies. Firstly, as mentioned in the previous chapters, is long recognized that Limestone and dolomite reservoirs constitute the largest source of supply of crude oil in the world (*Ericsson et al. 1998; Howard 1928; Hubbert and Willis 1955; Lucia 2007; Stearns and Friedman 1972*). Secondly, due to their genesis the mechanical properties of carbonate rocks are heterogeneous and different competence wants to be introduced in a multilayered system (*Twiss and Moores 1992*). Given these two observations, Limestone experimental data are collected and a difference of stiffness is imposed in order to characterize two types of rocks.

### 4.1 MACRO-SCALE PROPERTIES FROM LITERATURE

Focusing in Limestones rocks, experimental data are collected. Several unconfined compression test and triaxial test results were recorded for eight Limestone rocks (*Tsiambaos and Sabatakakis 2004*). All of them have been analyzed in order to identify the best Hoek-Brown failure data fitting. Taking into account the Hoek-Brown envelopes in *Figure 4.1* and the standard deviation of each data set (STD), reported below in *Table 4.1*, the micritic and the recrystalized micro-spartic limestone are selected and followed as a guide for the calibration of similar rocks. The experimental data of the two selected limestones are fully reported in Appendix A and graphically in *Figure 4.4* and *Figure 4.5* compared to the obtained numerical results. Due to the lack of data for tensile strength ( $\sigma_t$ ), these values are inferred from the Hoek-Brown envelope, recalling once again that this is acceptable given the purpose of use in the simulation admissible behavior of rocks. For the two limestone rocks, according to the numerical failure model reported in *3.4- Flat-*

Joint Model (FJM), the linear Mohr-Coulomb failure parameters are identified and the value of cohesion ( $c$ ) and friction angle ( $\phi$ ) are reported in Table 4.1.

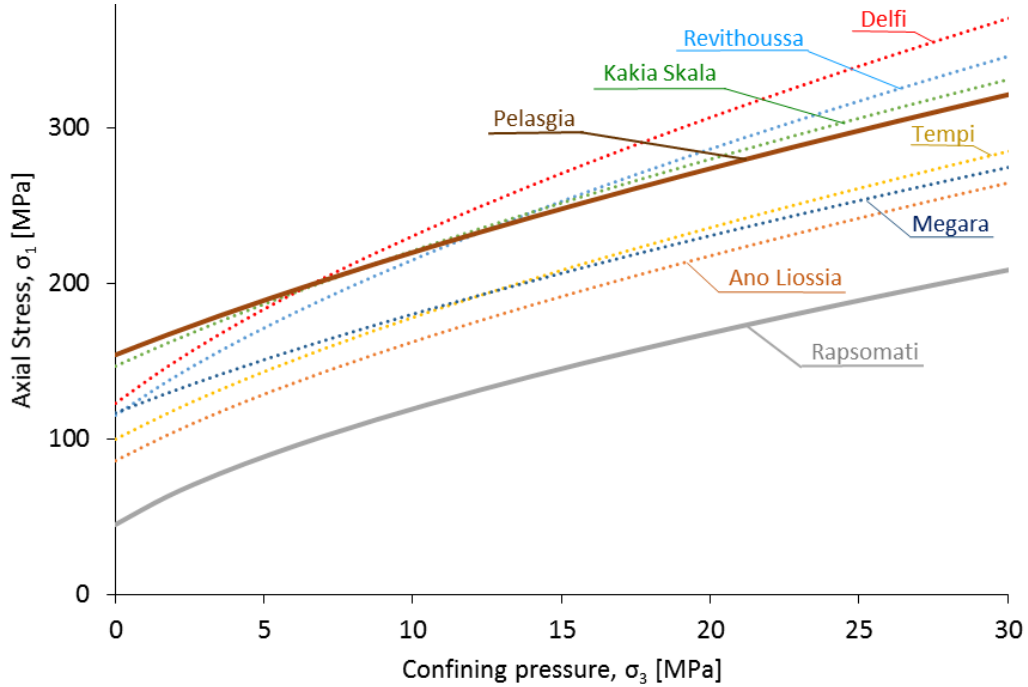


Figure 4.1: Hoek-Brown envelope of eight different Limestones. Data elaborated from (Tsiambaos and Sabatakakis 2004).

The obtained parameters are compared with several numbers of the test on different Limestone rocks performed and statistically interpreted (Sabatakakis et al. 2008). The results of 58 tests give a statistically based range of cohesion ( $c$ ) and friction angle ( $\phi$ ). The cohesion values range between 12MPa and 57 MPa with a mean of 31.82 MPa. The friction angle values range between 31 and 53 with a mean of 44.58. These results conform to results obtained from different authors (Barton and Choubey 1977; Jaeger et al. 2009; Patel and Shah) confirms the reliability of the obtained parameters, used for model the two types of rock.

Site	Rapsomati	Pelasgia
Type of Limestone	Micritic	Recrystallized micro-sparitic
STD	0.96	0.93
$\sigma_t$ [Mpa]	-2.03	-11.6
$c$ [Mpa]	$13.58 \pm 2.21$	$44.805 \pm 0.875$
$\phi$ [°]	$45.97 \pm 0.05$	$42.5 \pm 1.5$

Table 4.1: Standard Deviation (STD) and tensile strength ( $\sigma_t$ ) evaluated from Hoek-Brown envelope and values of cohesion ( $c$ ) and friction angle ( $\phi$ ) from analysis of data.

## 4.2 CALIBRATION OF MICRO-SCALE MODEL PARAMETERS

Based on literature limestone data the trial-and-error method is used to calibrate micro parameters of Flat-Joint contact model of rocks in PFC2D. An accurate explanation of the reasons for choosing this method and its description in the dedicate paragraph 3.4-Flat-Joint Model (FJM). In a DEM model, the mechanical properties of a specimen depend on the micro parameters defined at the particle level. The traditional calibration procedure (Itasca 2011) uses the deformability properties (Young's modulus and Poisson's ratio) and unconfined compressive strength (UCS) as the main matching properties, but must be noted that Itasca's guidelines provide suggestions on calibration of micro parameters only for contact bonded particle materials and parallel bonded-particle materials, therefore neglecting important aspects of the Flat-Joint Model (Chen ; Wu and Xu 2016).

### 4.2.1 Micro-scale parameters and their influence

Several papers on the effects of micro parameters on macro properties of specimens can be found (Boutt and McPherson 2002; Chen ; Fakhimi and Villegas 2007; Wang and Tonon 2010; Yang et al. 2006). The main micro parameters of a flat-jointed bonded particle material including particle parameters of particle density ( $\rho_s$ ), minimum particle radius ( $R_{min}$ ), particle radius ratio ( $R_{max}/R_{min}$ ), effective modulus ( $E_p$ ), normal-to-shear stiffness ratio ( $k_n/k_s$ ) and friction coefficient ( $\mu_p$ ) and flat-joint parameters: number of segments ( $N$ ), effective modulus ( $E_c$ ), normal-to-shear stiffness ratio ( $k_n/k_s$ ), friction coefficient ( $\mu_b$ ), radius multiplier ( $\lambda$ ), tensile strength ( $\sigma_b$ ), cohesion ( $c_b$ ), and friction angle ( $\phi_b$ ) or internal friction coefficient ( $\tan\phi_b$ ). Through the calibration literature and the parametric studies, the main influences of micro parameters on macro properties are summarized in Table 4.2 (Chen ; Wu and Xu 2016). The influence of micro parameters is shown by the average coordination number (CN), the crack density (CD), bond cohesion, the tensile strength and local friction angle. To be consistent with the dimensionless Unconfined Compression over Tensile Strength ratio (UCS/TS) the bond cohesion and tensile strength are treated as one parameter ( $c_b/\sigma_b$ ). The other macro properties influenced are the Hoek-Brown strength parameter ( $m_i$ ) and the friction angle ( $\varphi$ ).

		<i>Coordination Number CN</i>	<i>Crack Density CD</i>	<i>Bond cohesion over tensile strength ratio <math>c_b/\sigma_b</math></i>	<i>Local friction angle <math>\phi_b</math></i>
<i>Unconfined Compression over Tensile strength ratio</i>	UCS/TS	+	-	+	
<i>Hoek Brown strength parameter</i>	$m_i$	-	+	+	+
<i>Friction angle</i>	$\phi$		+	+	+

Table 4.2: Influence of micro parameters on macro properties.

Furthermore, is also well recognized that the residual friction angle in Flat-Joint Model has only a little influence, on all the three macro parameters, and mainly influences post peak behavior (Wu and Xu 2016). From the analysis in Chen (year),  $E$  is shown to be dependent on  $k_n/k_s$  and  $E_c$  (Chen).

#### 4.2.2 Test procedures

The characterization of rocks has been done running unconfined compression, tensile and biaxial, with different confining pressures, tests on the specimens reported in *Figure 4.2*. In the limestone uniaxial compression PFC2D model, the particle aggregations are 100 mm high and 50 mm wide. Each specimen is set with walls (friction coefficient = 0) at lower and upper ends, and assigned with axial stress exerted at constant rates of similar sizes and opposite directions (*Figure 4.2a*). In the limestone direct tensile PFC2D model the particle aggregations are 100 mm high and 50 mm wide. A thickness of approximately 7-8 layers of grains is defined at both ends of the specimen as the gripped portion, through which the specimen is pulled apart (see *Figure 4.2 (b)* ). Each specimen is also subjected to biaxial test with confining pressure of 10 MPa and 20 MPa applied to lateral rigid frictionless walls (*Figure 4.2c*). The loading or expanding velocity is controlled slow enough so that the specimen remains in quasi-static equilibrium during the loading process.

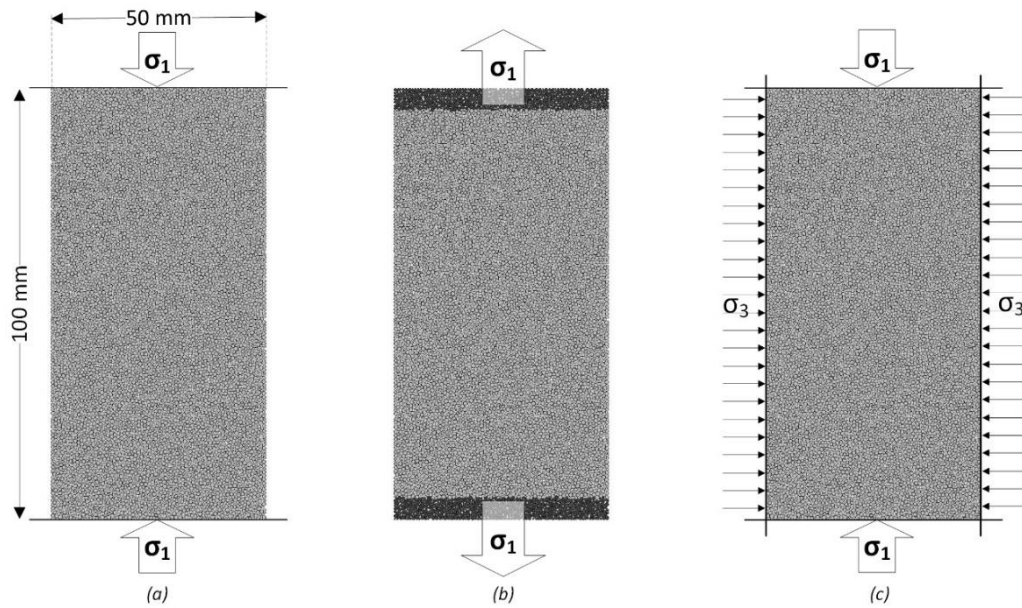


Figure 4.2: Specimens for (a) Unconfined Compressive test, (b) direct tension test and (c) Biaxial test.

### 4.2.3 Calibration procedures

Through the literature reported experience of calibration and previous parametric study, the influence of micro parameters to macro properties is taken into account and the trial-and-error method is used to calibrate micro parameters. Before to follow the flowchart, of the mentioned method, reported below in *Figure 4.3*, the equivalent input micro parameters are calculated through the equation suggested in literature (*Chen*). During calibration of micro parameters,  $\rho_s$  is assumed to equal to  $2500 \text{ kg/m}^3$ , according to common limestone density values, and a maximum to minimum grain radius is fixed to 1.66 for both rocks.

Micro parameters			Rock type 1	Rock type 2
Effective modulus of both particle and bond	$E_p = E_c$	[GPa]	50.00	20.00
Ratio of normal to shear stiffness of both particle and bond	$k_n/k_s$	[-]	2.20	2.60
Bond tensile Strength	$\sigma_b$	[MPa]	15.00	2.76
Bond cohesion strength	$c_b$	[MPa]	60.00	18.61
Local friction angle	$\varphi$	[°]	8.00	17.00
Residual friction coefficient	$\mu$	[-]	0.40	0.30

Table 4.3: Micro-scale parameters of characterized rock types.

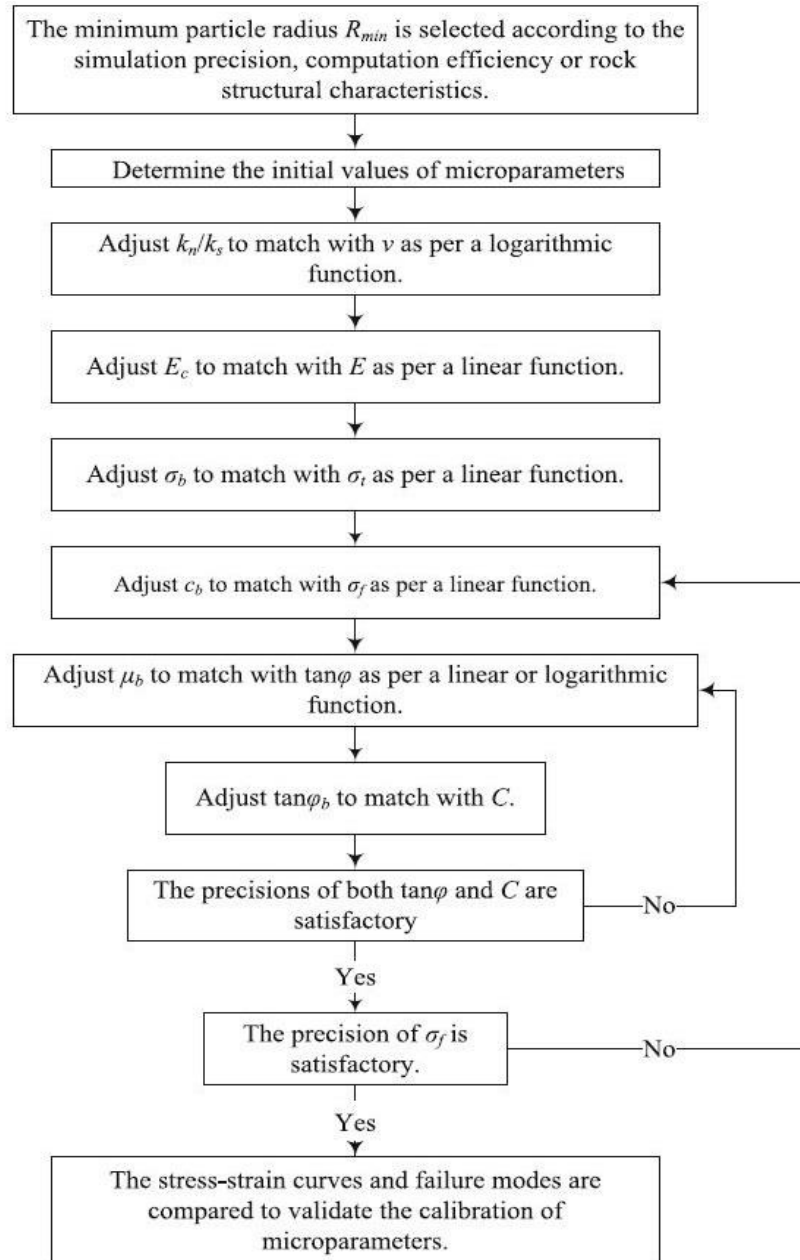


Figure 4.3: Trial-and-error calibration procedure flow-chart, modified after (Chen).

### 4.3 CALIBRATION RESULTS

In the end, the bound and particle parameters used for the calibration are summarized in *Table 4.3*. The rock type 1 is characterized following the recrystallized micro-sparitic limestone from Pelasgia site. Meanwhile, the rock type 2 is referred to micritic limestone from Rapsomati. The data from literature and the obtained strength for different confining pressures are plotted below for both rock types with relative guide limestone.

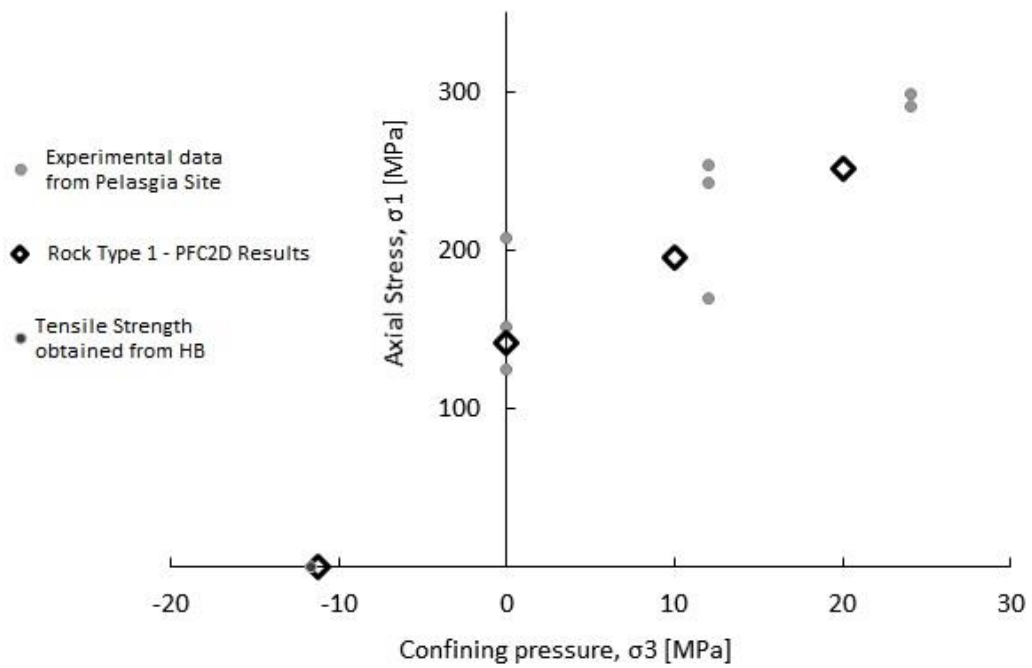


Figure 4.4: Results of tests for the calibration of Rock Type 1.

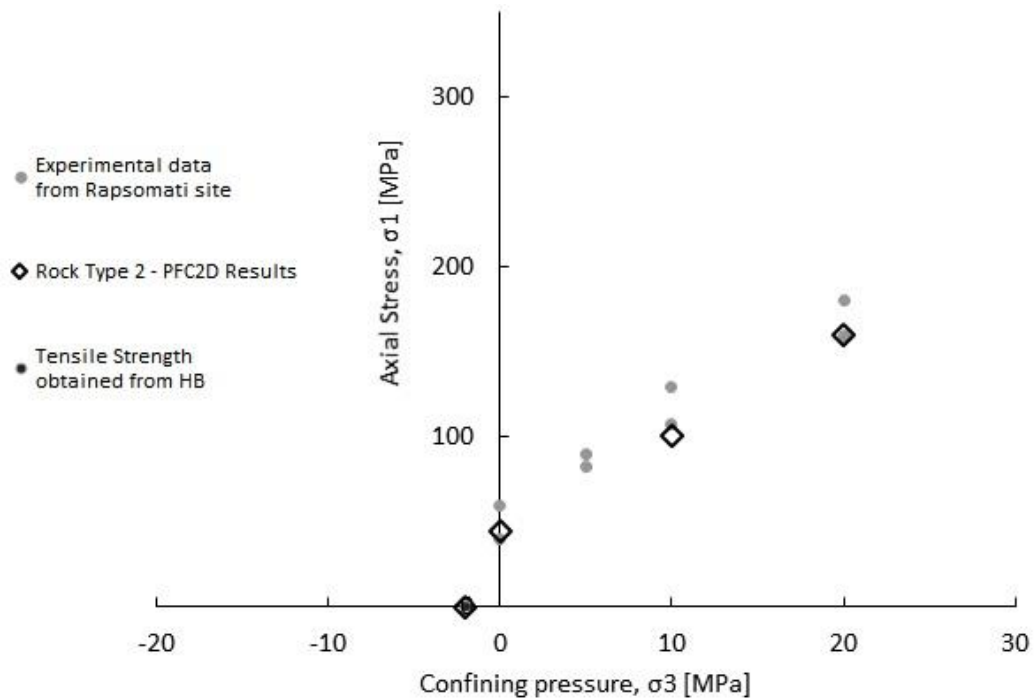


Figure 4.5: Results of tests for the calibration of Rock Type 2.

The Young's Modulus, as macro properties, for the two rocks types is evaluated equal to 56 GPa for the first and 21.9 GPa for the second rock type.

## **4.4 INTRODUCTION TO ROCK MASS MODELING (SYNTHETIC ROCK MASS)**

For the aims of this paper intact rock is calibrated in order to appreciate the fracture development, in brittle rock, only during the folding process. It must be noted that, at the scale taken into account, rock mass should be modeled. Rock mass consists of block rocks and complex discontinuities, which makes the rock mass weaker, more deformable, more heterogeneous compared to intact rock. It is difficult to completely understand the mechanics of rock mass, as even within a single rock type designation zone, its deformability and strength behaviors can differ (*Mogi 2007*). Because the laboratory experiments and in situ tests are time-consuming and expensive, numerical simulation has proven to be a new avenue for obtaining the mechanical behaviors of geo-materials. The combination of bonded contact models to capture the behavior of intact material with the SJM for joint network leads to the development of the so-called synthetic rock mass (SRM) (*Ivars et al. 2011*), which aims at numerically predicting rock mass properties, including scale effects, anisotropy and brittleness, that cannot be obtained using empirical methods. SRM samples containing thousands of non-persistent joints can be submitted to standard laboratory tests (UCS, triaxial loading, and direct tension tests) or tested under a non-trivial stress path representative of the stresses induced during the engineering activity under study. Overall, the SRM approach provides a basis for the development of a rational framework for estimation of rock mass deformation, strength, and brittleness and should be used routinely to supplement empirical estimates.

## 5 BOUNDARY CONDITIONS IN ANTICLINE STUDIES

---

The influences of different boundary conditions and different folding mechanism are investigated in this section. The aims are to figure out the boundary condition influences of each model setup and the relative ensuing fractures. The results shown below are intended to be a tool for identifying the most suitable features and boundary conditions for future tests. Two main mechanisms are investigated to simulate the anticline formation, layer-parallel shortening and bending. Pre-modelling analysis is presented to avoid mechanical instability and have a better understanding of the mechanism that occurs in layer-parallel shortening.

### 5.1 PRE-MODELLING ANALYSIS

Dimensionless analysis is proposed as tool to model the initial shape of a buckled anticline to give a certain degree of confidence regarding the physic reliability for the chosen buckled shape. The analysis has been developed on a single homogeneous layer of intact rock. Rheological and time depending factors were not taken into account. The main influencing parameters considered are the layer Young's Modulus (E) and the Unconfined Compression Strength (UCS), the principal layer-parallel stress ( $\sigma_1$ ) and slenderness ( $\lambda^2 = \frac{12 \cdot L^2}{h^2}$ ). Looking for a range of stress and slenderness where buckling without shear failure is allowed, through the Euler's critical force the stress required to buckle is obtained,  $\sigma_{cr} = \frac{\pi^2 E}{\lambda^2}$ . Two dimensionless parameters are introduced, the *stress ratio*  $\gamma = \frac{\sigma_1}{UCS}$  and the *slenderness ratio*  $\Lambda = \frac{\lambda}{\lambda_c}$  where  $\lambda_c$  is the slenderness associated with buckling. Must be noticed that for  $\gamma=1$  the shear failure is reached increasing the layer-parallel stress meanwhile buckling is achieved for  $\gamma = \frac{1}{\Lambda^2}$ . In absence of upper layer, tre different mechanism can be appreciated. For slenderness ratio in the range  $0 < \Lambda < 1$  only shear failure is allowed. For slenderness ratio equal to 1 shear failure and buckling occur simultaneously when the stress applied is equal to the unconfined compression strength. For values greater then one buckling occur followed by shear failure increasing the axial stress.

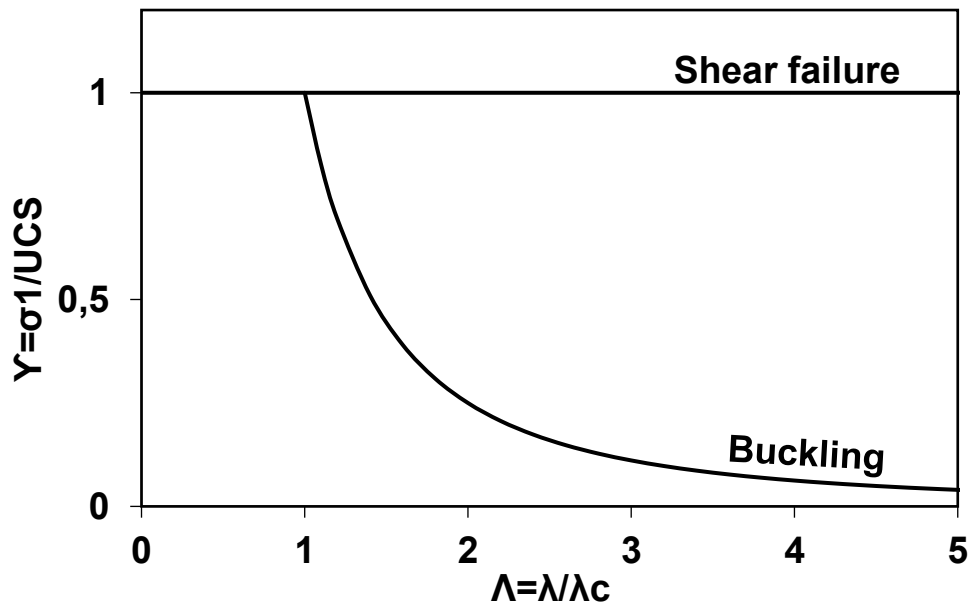


Figure 5.1: Dimensionless plot of layer-parallel behavior.

Pre-modelling analysis has also been developed in order to take into account the *burial depth*. Two main mechanisms are identified depending on the dimensionless parameter defined as burial depth over layer thickness ratio ( $H/h$ ), also called thickness ratio. The mechanisms are studied with the aim of identify what aspects are essential for the models and find analytical expression of the buckling domain. Shallow anticline related mechanism is studied for ratio value lower than 0.1. In this case the upper layer exerts a confining pressure that is opposed to the natural inflection of the considered anticline, following its deformation. The Shallow anticline is studied as elastic beam buckling problem with uniform distributed and inflection imposed opposite to the distribute load direction. Deeper, the mechanism can be associated to anticline in weaker matrix for thickness ratio higher than 10. In this latter case the upper layer only absorbs the anticline deformation, without inflection on the surface. This latter mechanism is modeled as elastic foundation above the elastic beam. For different thickness ratio order of magnitude the combination of these two main mechanism must be considered.

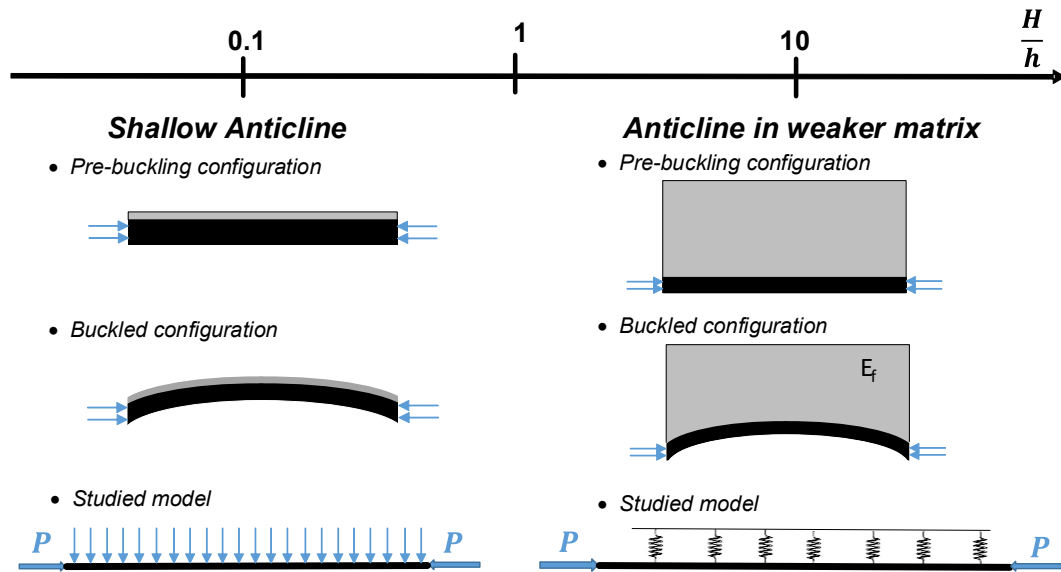


Figure 5.2: Burial depth related mechanism depending on thickness ratio between burial depth and layer thickness ( $H/h$ ).

Once figure out the essential geology aspect of the model, the boundary conditions can be designed. For shallow anticline, the layer-parallel shortening presented below can be associated with flexible membrane to apply confining pressure. Meanwhile, to simulate anticline in weaker matrix, this latter boundary condition cannot be applied. The proposed boundary conditions to model deeper anticlines consist of an anticline surrounded by frictionless grains with lower stiffness were the lithostatic pressure can be applied through rigid wall or flexural membrane on the confining grains while the layer parallel shortening can be applied similarly to the unconfined case reported below.

## 5.2 LAYER-PARALLEL SHORTENING

The buckling folding mechanism is reported in 2.1.2 - Folding mechanisms. In a mathematical sense, buckling is a bifurcation in the solution to the equations of static equilibrium. At a certain point, under an increasing load, any further load is able to be sustained in one of two states of equilibrium: a purely compressed state or a laterally-deformed state. The anticline formation, for this mechanism, is studied designing the model in a buckled configuration to avoid the difficulties to reproduce and manage mechanical instability in codes based on discontinuum assumption.

### 5.2.1 Models

The results of pre-modelling analysis has been used to avoid mechanical instability simulating pre-buckled anticlines. A critical slenderness value ( $\Lambda=2$ ) is used to have a reasonable range of buckling deformation before to reach the shear failure. No higher values are used to have a low slenderness for particles number optimization. For given length, higher thickness will be designed with ensuing greater number of particles. For all the models a particle-based approach is used. Fixed the critical slenderness value the pre-buckled anticline geometry is defined as reported in *Figure 5.3*. The layer-parallel shortening is applied by rigid walls with speed of 0.005 m/s. Firstly the influence of boundary conditions is investigated. Simulation results from *affected domain* test and *extended domain* test, of pre-buckled anticline, are compared. The extended domain model differs from the affected domain for an additional non-curved length in the ending parts. Indeed, 15'321 particles are used for the affected domain. Meanwhile, 18'848 particles are used in the extended domain. For both the models the “rock type 1” characterized before is used.

The extended domain is also used in *multi-layer model* simulation to investigate the fracture evolution and mechanical behavior. The geometry is defined by keeping the same slenderness ratio ( $\Lambda=2$ ) for each of the two stiffer layers (rock type 1) above and below a weaker layer (rock type 2). The weaker layer have the same geometry of a single layer with different rock properties, consequently different critical slenderness ratio. The layers are cemented together. The number of particles used for the multi-layer model tested is 27'825, equally distributed in the three layers.

### 5.2.2 Results

The influence of boundary conditions and initial shape on fracture evolution is investigated for single layer models. The global stress-strain curve is compared with the number of partial cracks evolution. The number of partial cracks is used since applying the contact model (Flat-Joint Model) the bonded interface is discretized in three elements and each single breakage is recorded. Both the models presents a global shear failure associated to a global stress drop-off consistent with a sharp

increase in a number of partial cracks, followed by a plateau. In the affected domain the anticline tends to reduce its slenderness under the layer-parallel shortening mechanism until the global shear failure is reached, as shown by force chain evolution plots *Figure 5.5*. The boundary conditions hinder the natural deformation of the anticline as we can see looking at the fracture network immediately before and after the global shear failure. Once the global failure is reached on the contact with rigid walls, the tensile fracture network develops. The global axial stress increases almost linearly until the global shear failure. The associated partial crack evolution presents a slight increasing getting closed to the global shear failure. The additional tensile-breakable lengths introduced in this latter model allows the natural tensile fracture development even before the global failure. Accordingly, the total number of partial cracks is higher and the main effect is that the global stress peak is preceded by a smooth decrease. Therefore, to allow the natural evolution of fracture network and avoid the limitation related to the contact anticline-wall an extended domain has been taken into account.

Using extended domain a multi-layer mechanical unit is subjected to layer-parallel shortening. As expected the weaker layer reaches the failure before the two stiffer layer. The shear failure of a single layer strongly affect the surrounding layers. The global axial stress presents a linear increasing until the peak where the global shear failure is reached followed by a drop-off that, unlike the single layer, is characterized by two main slopes. As shown in the fracture evolution and force chain plots, as the shear failure is reached, detachment occurs between the top layer and the layers below. Even if the top layer behaves as single layers, the fracture evolution is strongly controlled by the bottom fracture network. This stage of fracture evolution, related to the only top layer, controls the second slope of global stress evolution before to reach the zero global stress and the partial cracks plateau.

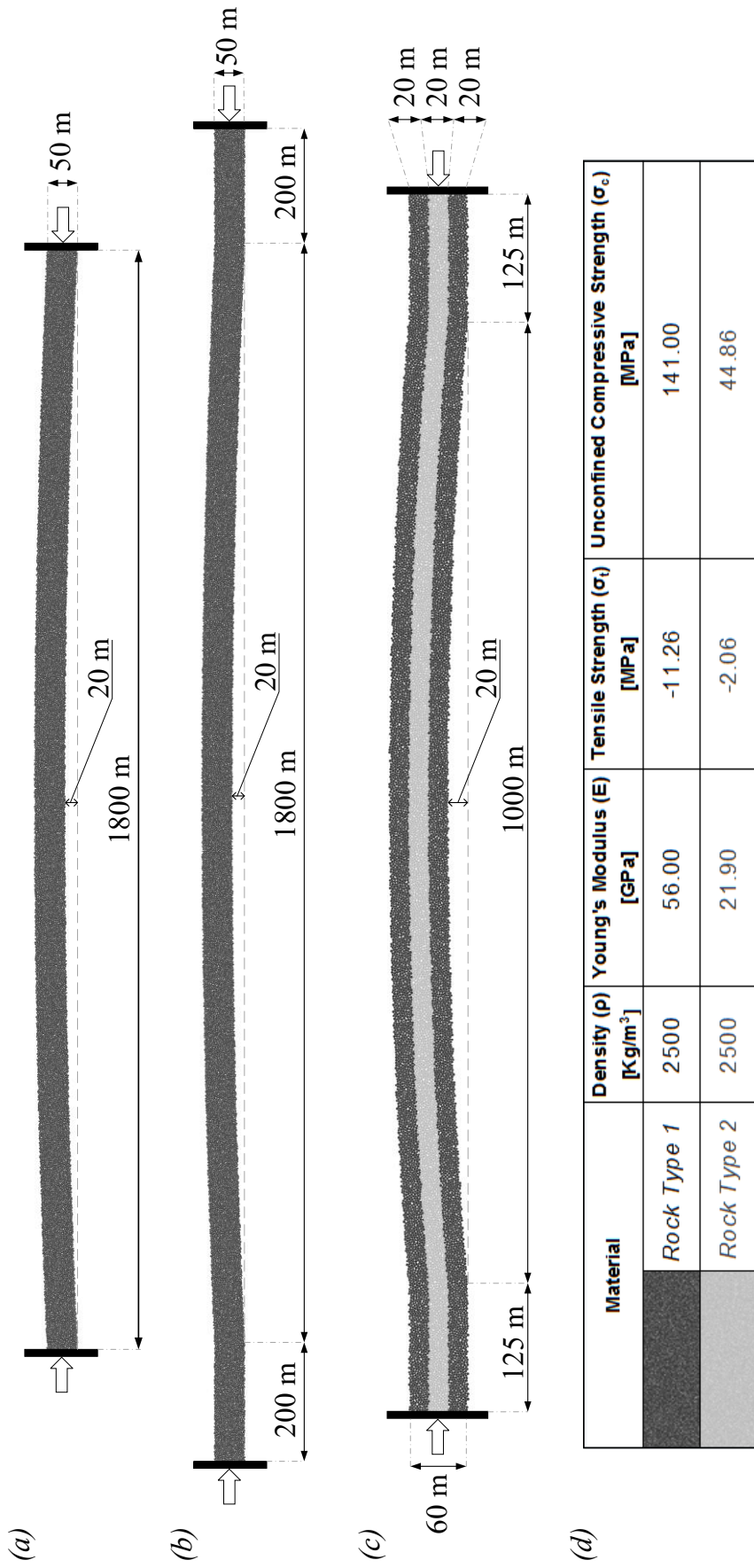


Figure 5.3: Layer-parallel shortening: (a) Affected domain single layer model; (b) Extended domain single layer model; (c) Multi-layer model; (d) Table of used rocks.

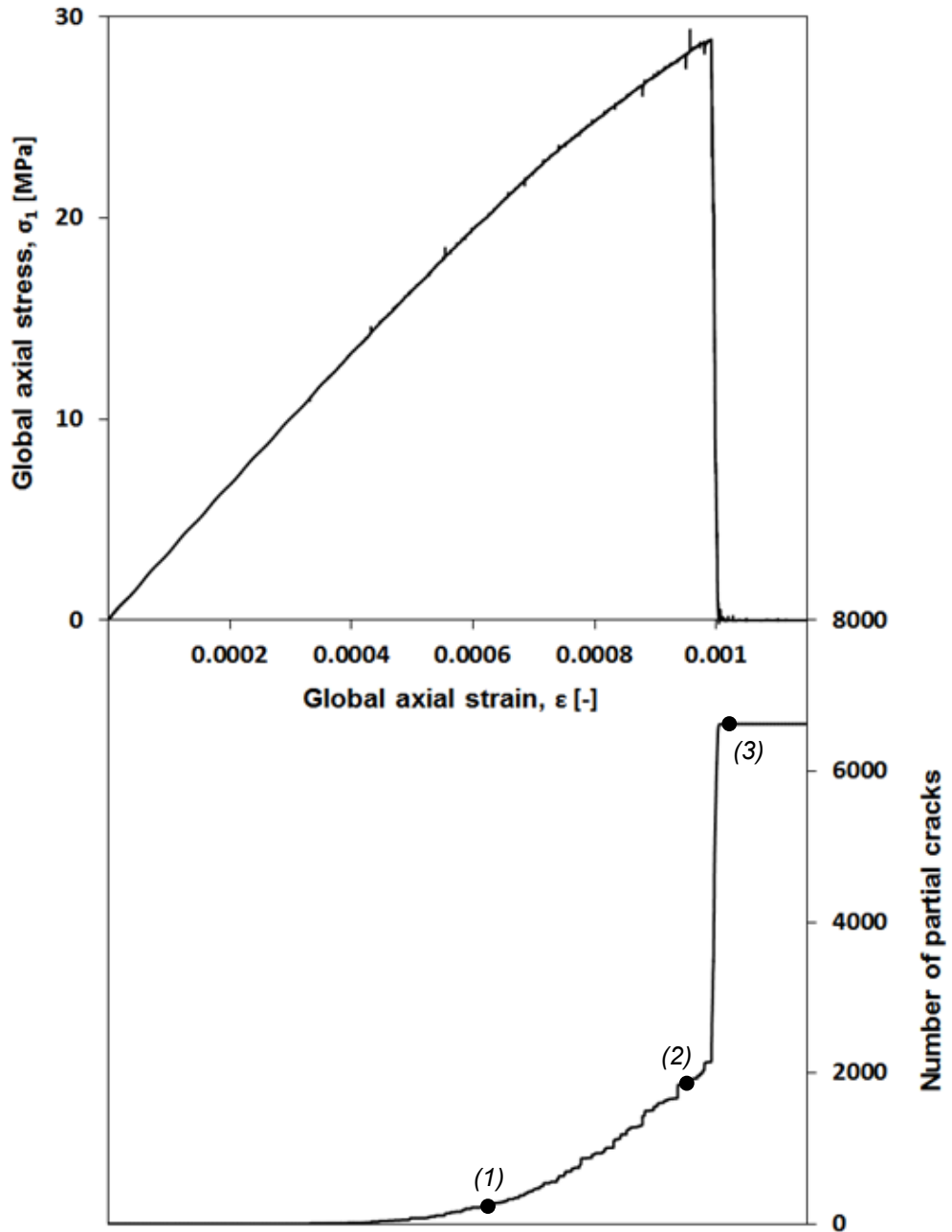


Figure 5.4: Layer-parallel shortening results of affected domain single layer model - Global axial stress-strain curve and number of partial cracks evolution.

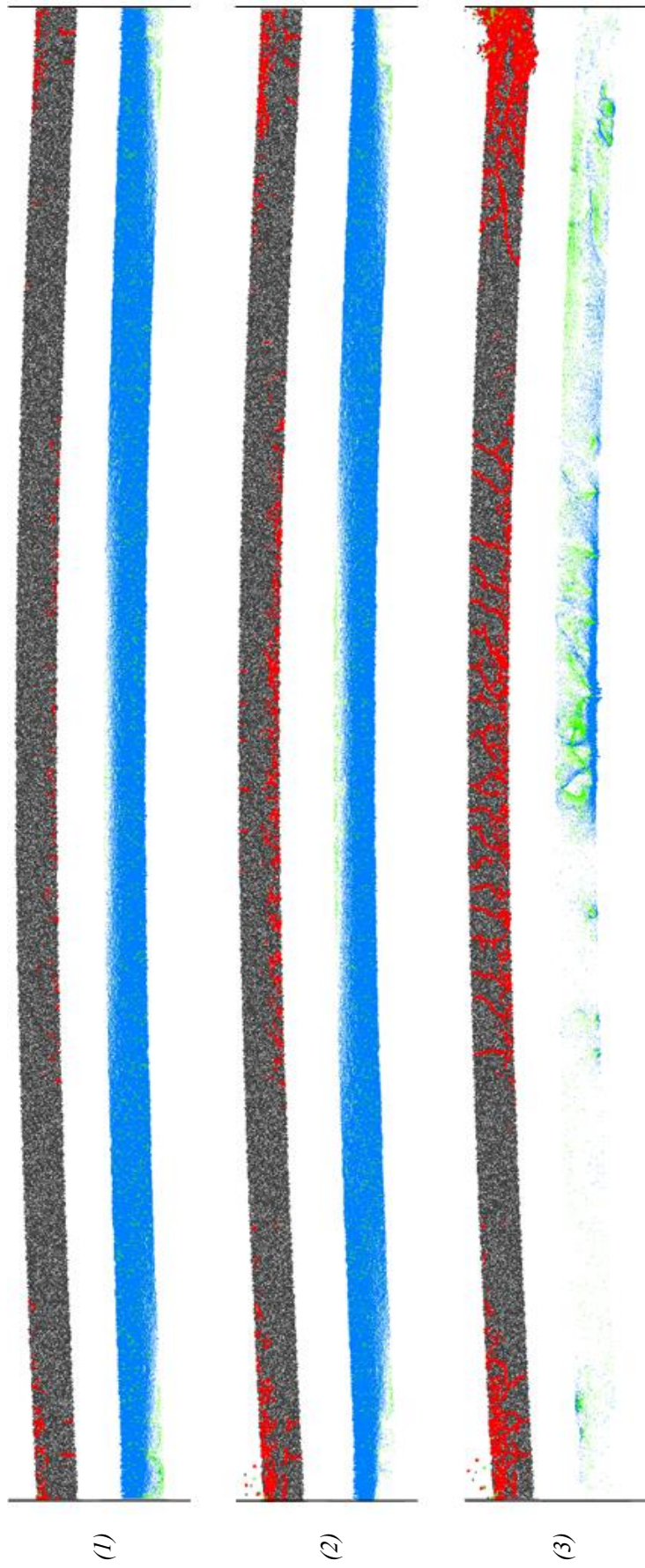


Figure 5.5: Layer-parallel results for affected domain single layer model - fracture state on the top and force chain on the bottom, of each pair, for steps (1), (2) and (3) defined in "Figure 5.4".

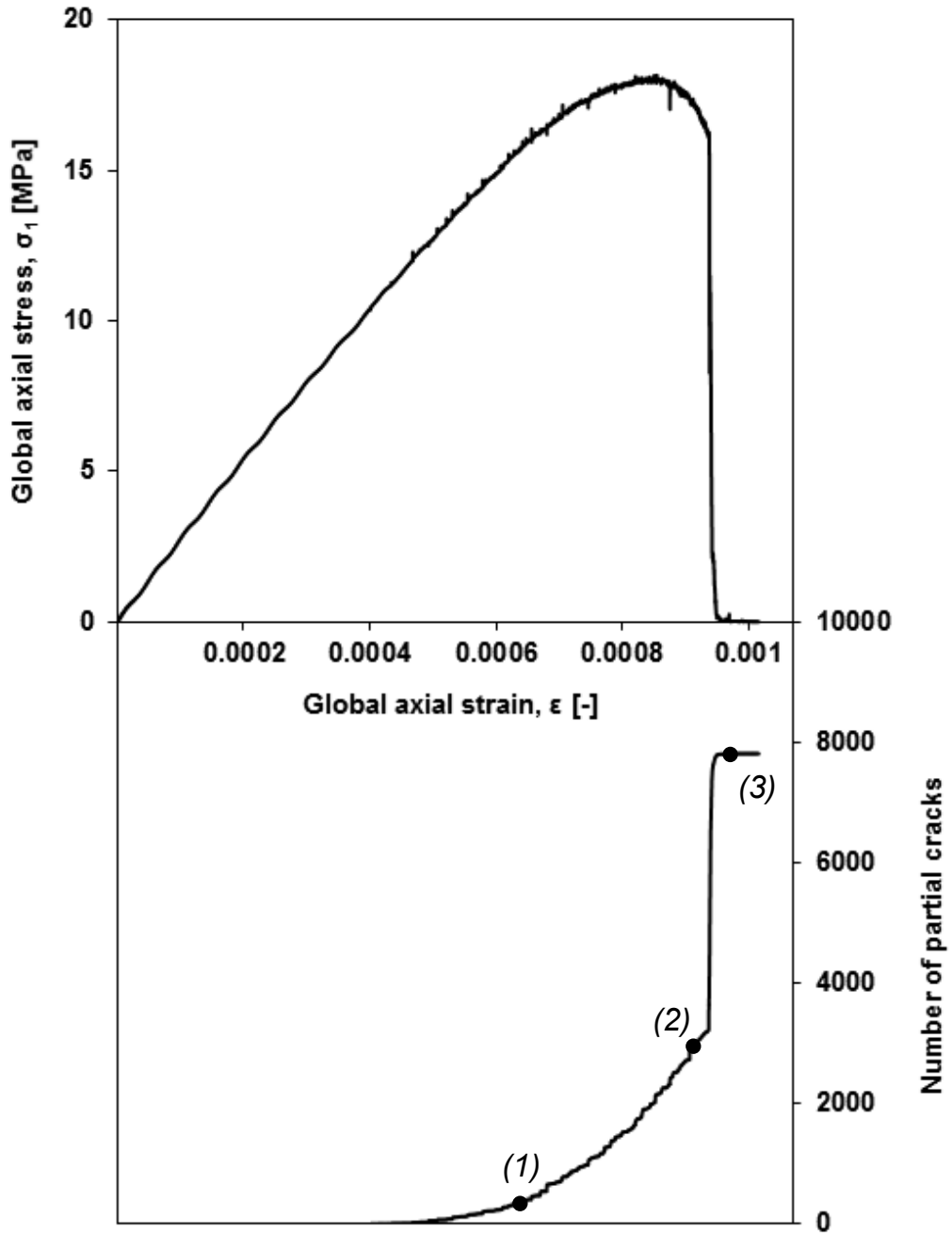


Figure 5.6: Layer-parallel shortening results of extended domain single layer model - Global axial stress-strain curve and number of partial cracks evolution.

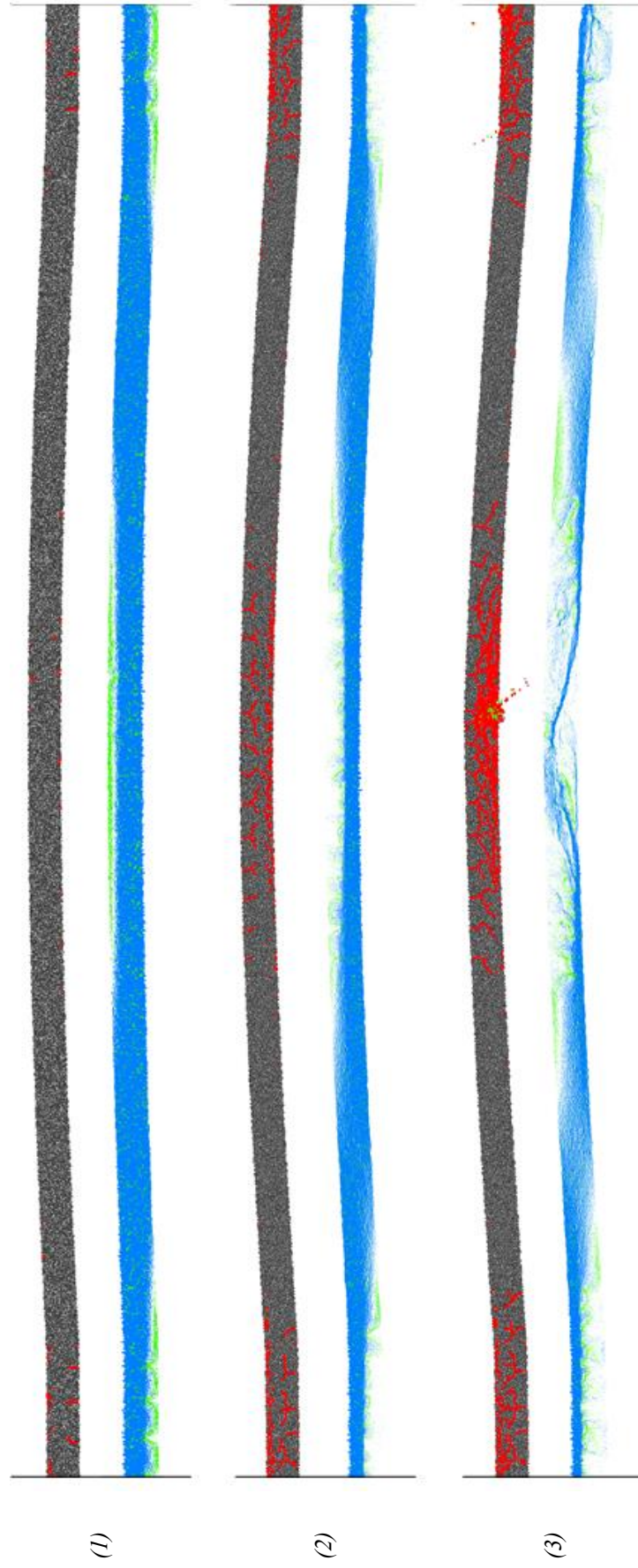


Figure 5.7: Layer-parallel results for extended domain single layer model - fracture state on the top and force chain (where blue indicates compression and green tension) on the bottom, of each pair, for steps (1), (2) and (3) defined in “Figure 5.6”.

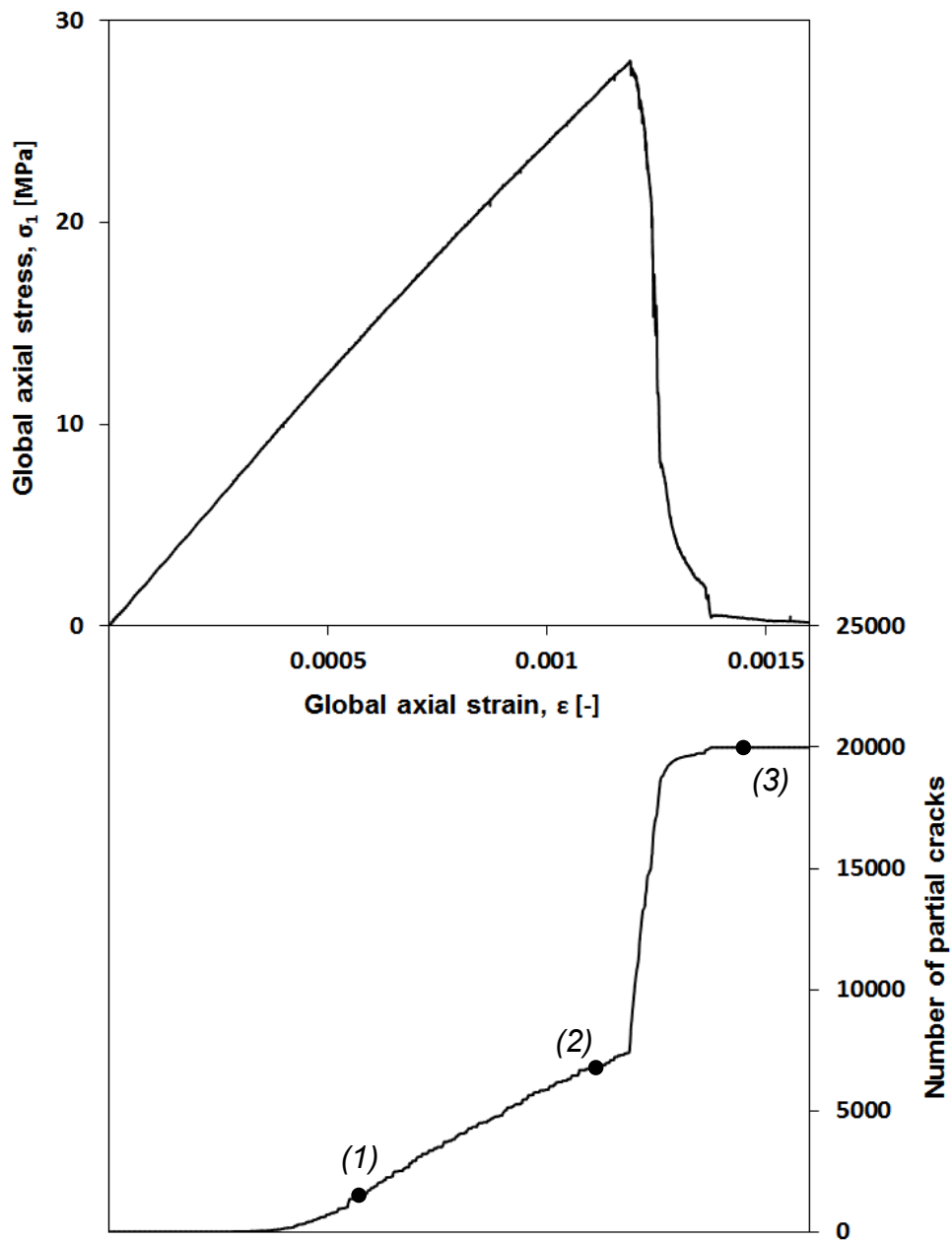


Figure 5.8: Layer-parallel shortening results of extended domain multi-layer model - Global axial stress-strain curve and number of partial cracks evolution.

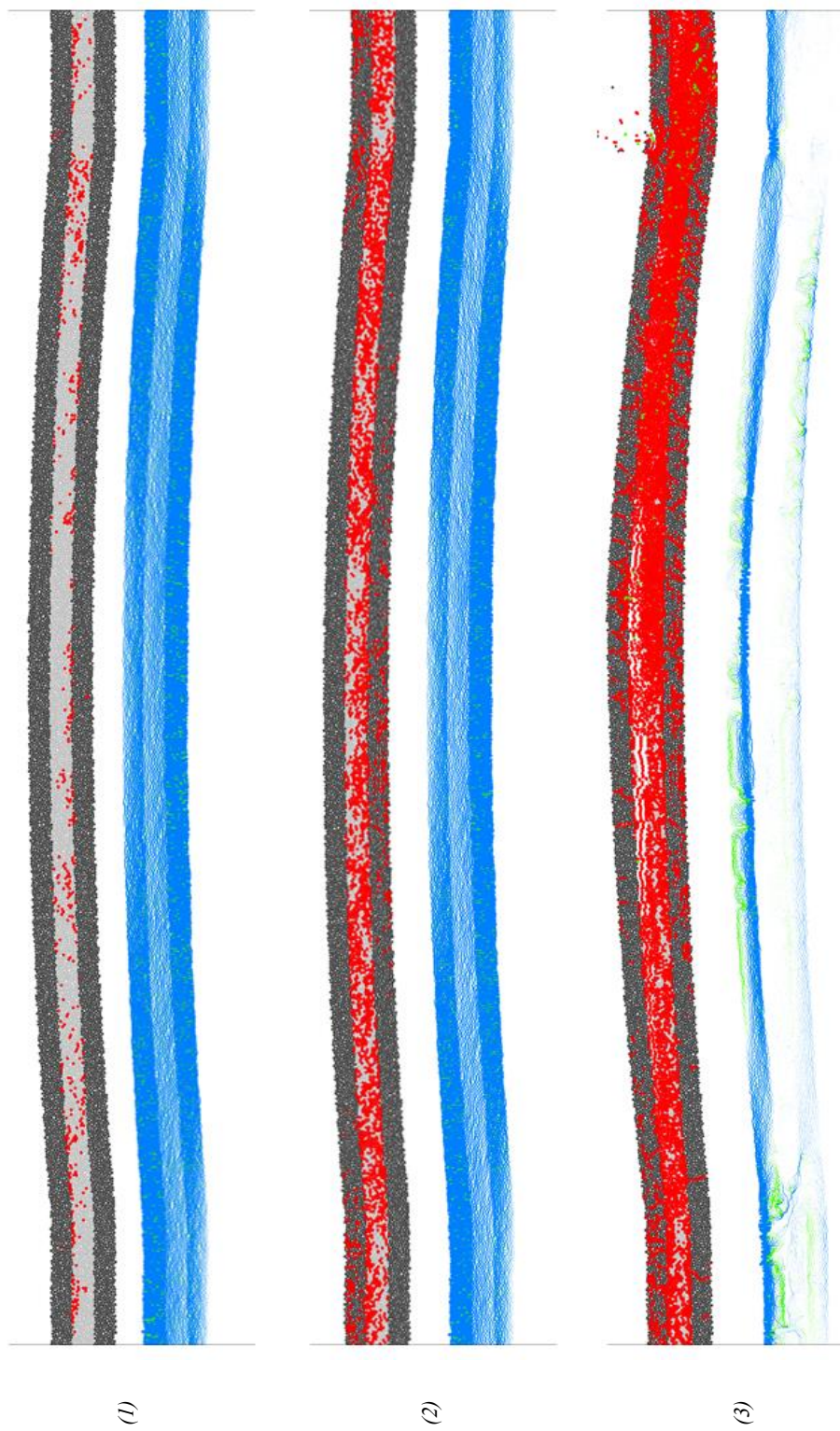


Figure 5.9: Layer-parallel results for extended domain multi-layer model - fracture state on the top and force chain (where blue indicates compression and green tension) on the bottom, of each pair, for steps (1), (2) and (3) defined in “Figure 5.8”.

## **5.3 BENDING**

The buckling folding mechanism is reported in 2.1.2 - Folding mechanisms. For this loading processes the pre-modelling analysis presented above is not taken into account since bifurcation of static equilibrium is not present.

### **5.3.1 Models**

A multi-layer system is designed in order to compare different loading process. Same geometry and properties of the affected area from layer-parallel shortening, presented above, are used. The same global geometry is also used in a single layer simulation to investigate the influence of boundary conditions in the associated fractures evolution. The comparison of these two results allow us to investigate how, for given geometry, the presence of a weaker layer in a stiffer matrix influence the behavior of a mechanical unit in the anticline formation. The bending folding mechanism is simulated by rotation of rigid walls around its center. The velocity applied is 0.0005 degrees/s. The anticline is not cemented with the wall. This latter assumption is physically reliable since applying the same stress in compression, on the bottom, and in tension, on the top, the upper part will break quiet immediately the contact while the compression stress increase keeping the contact.

### **5.3.2 Results**

Different fracture evolution are shown comparing different loading process. The single layer result shown the influence of imposed boundary conditions on the fracture network. The loss of contact wall-anticline, associated with the development of macro tensile fracture on the top of the layer, influences the stress neutral surface that strongly controls the fracture bifurcation. The global stress-strain curve is compared with the number of partial cracks evolution. The number of partial cracks is used since applying the contact model (Flat-Joint Model) the bonded interface is discretized in three elements and each single breakage is recorded. The local slope of number of partial cracks curve is strictly related to the onset of macro tensile fracture, that can propagate easily compared to compression related fractures, and to the interaction and connectivity of fractures. As expected, concurrently with anticline-wall contact moment drop-off, the stronger slope

variation is recorded and consequently a sharp increase of number of partial cracks. The rate of cracks generation decrease reaching the moment inflexion point, mostly related to the bifurcation propagation. Afterwards another slope change is related to the interaction and propagation of fracture that forms from previous fractures bifurcations.

The main results obtained from bending loading process comes from the multi-layer simulation. The initial fractures take place in the weaker layer from the boundaries, developing through the layer. The second fracture evolution stage starts when the propagation of this almost layer-parallel fractures stopped. This stage can be identify in the number of partial cracks-wall rotation curve for rotation between 1 and almost 2.8 degrees. The presence of this two main fractures induce a clear discontinuity in the displacement field between either sides of the fractures. The severity of the discontinuities decreases towards the center until again reaching a state of homogeneity, until the onset of macro tensile fractures and relative bifurcations leads the fractures to connect. In the end, during the last states the contact moment evolution presents an anomaly from the continuum decrease trend characterized by sharp drop-off and increase until zero contact moment is reached. During this last step while the first fractures are blocked by the interface between weaker and bottom stiffer layer, the latest fractures propagates through this interlayer.

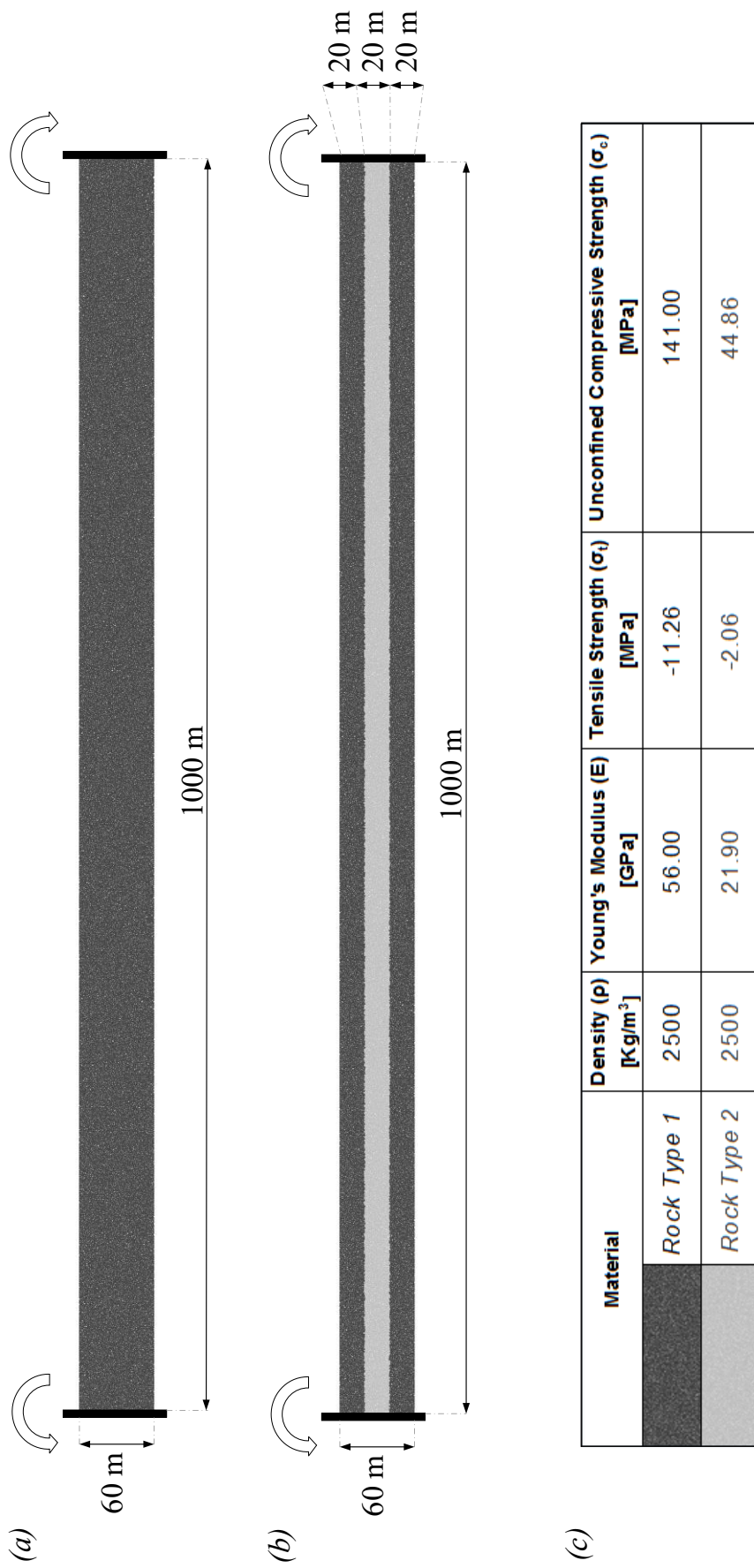


Figure 5.10: Bending: (a) Single-layer model; (b) Multi-layer model; (c) Table of used rocks.

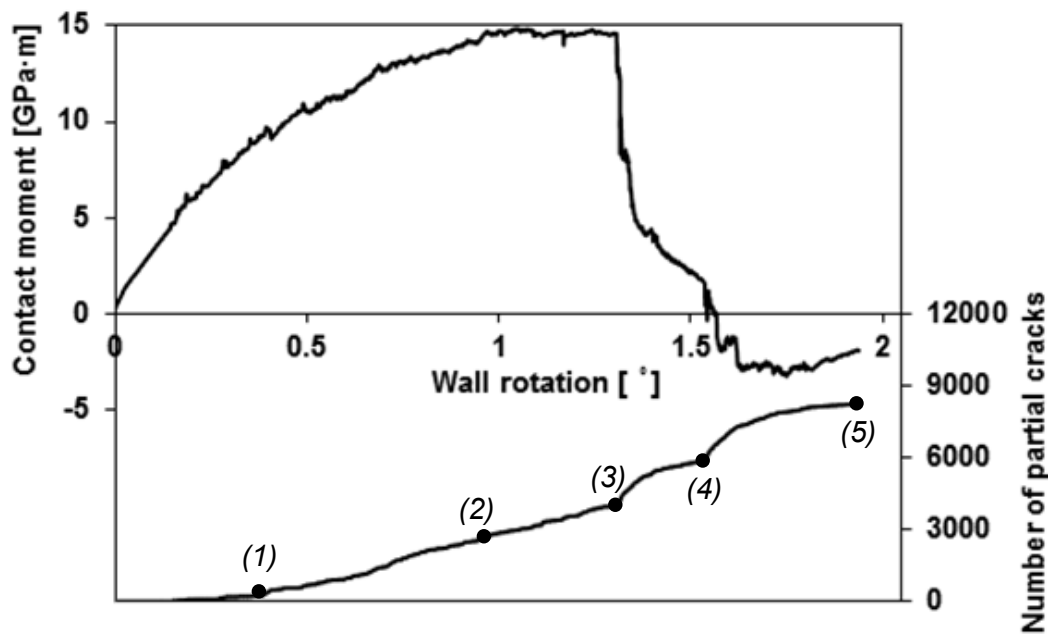


Figure 5.11: Bending results of single layer model - Global axial stress-strain curve and number of partial cracks evolution.

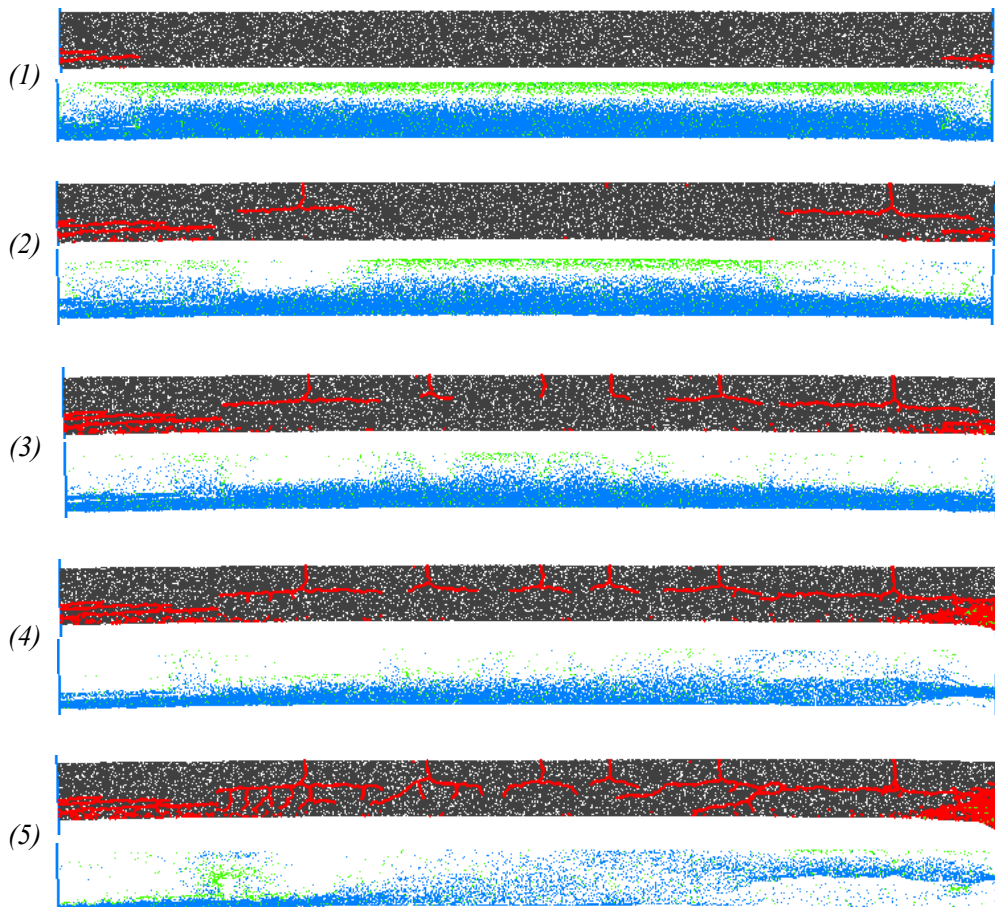


Figure 5.12: Bending single layer model - fracture state on the top and force chain (where blue indicates compression and green tension) on the bottom of each pair, for steps (1), (2), (3), (4) and (5) defined in "Figure 5.11".

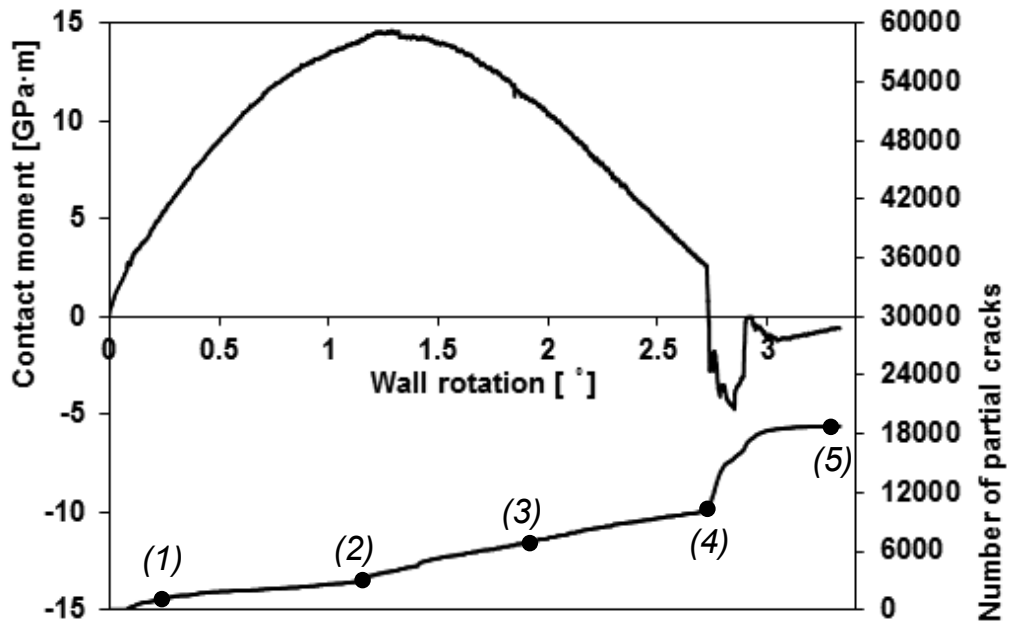


Figure 5.13: Bending results of multi-layer model - Global axial stress-strain curve and number of partial cracks evolution.

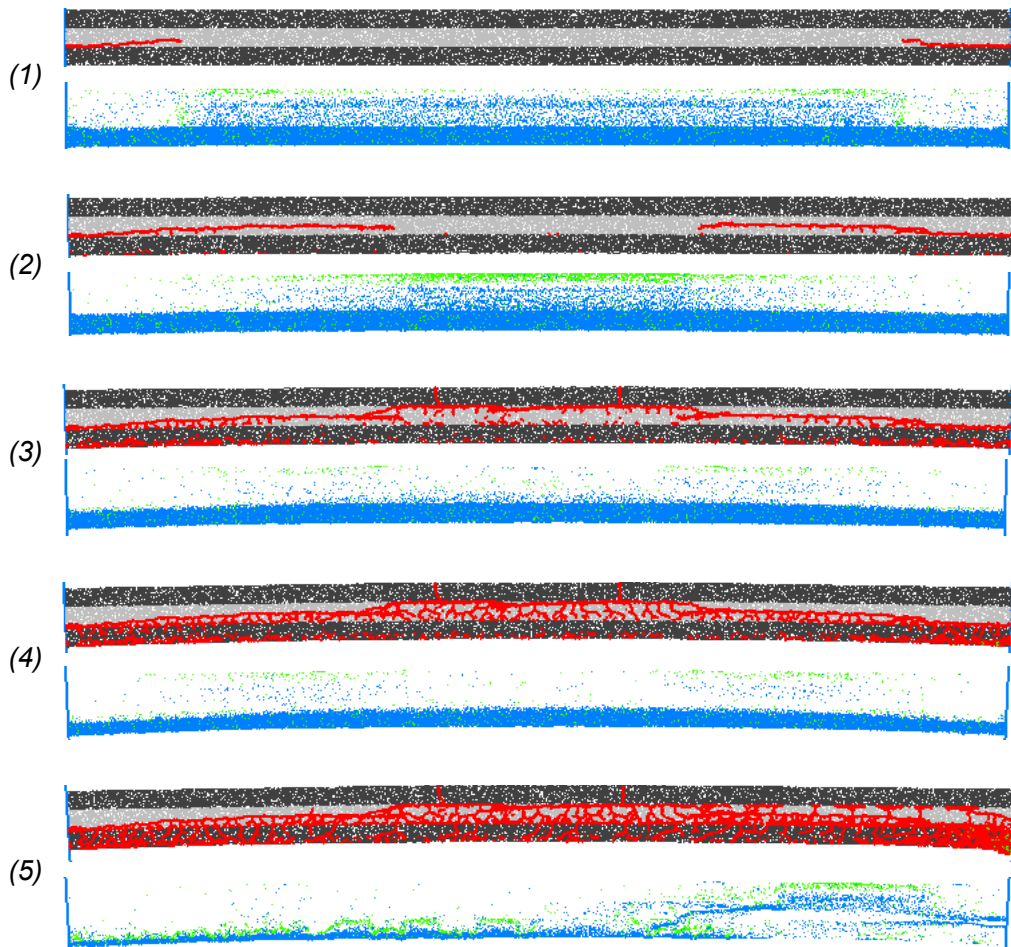
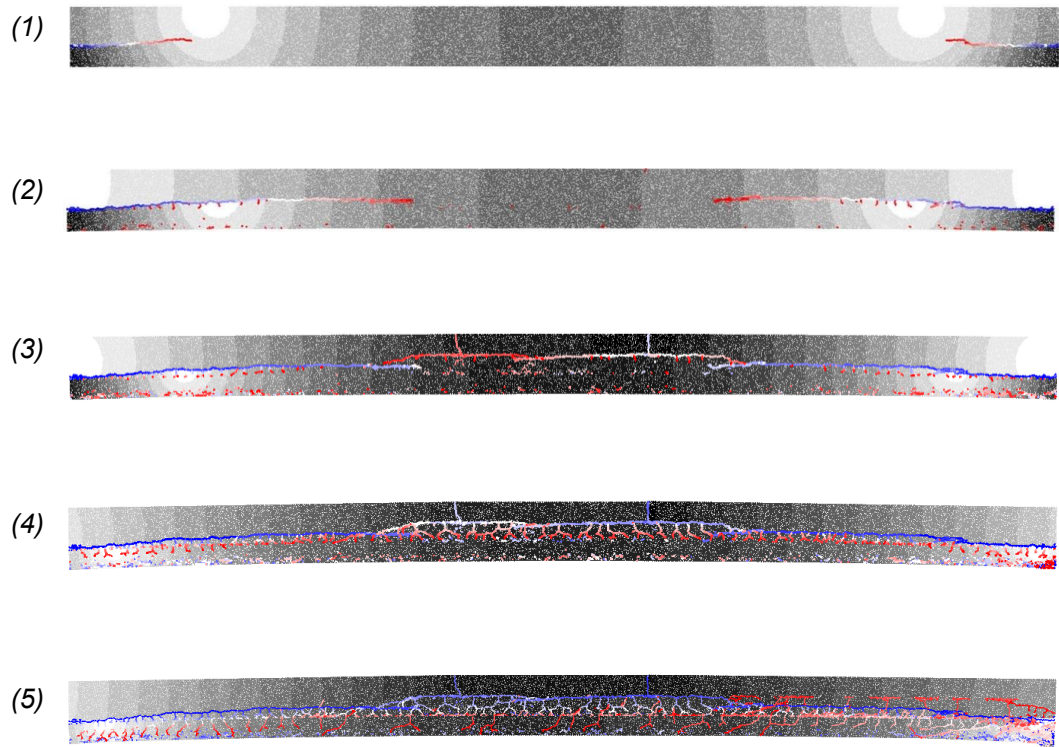
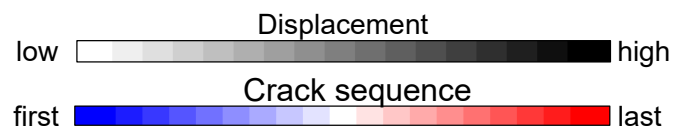


Figure 5.14: Bending multi-layer model - fracture state on the top and force chain (where blue indicates compression and green tension) on the bottom of each pair, for steps (1), (2), (3), (4) and (5) defined in "Figure 5.13".



*Figure 5.15: Bending multi-layer model – Displacement field and crack sequence for steps (1), (2), (3), (4) and (5) defined in “Figure 5.13”.*

## 6 CONCLUSIONS

---

The Discrete Element Method (DEM) allows us to overcome several limitations of the previous methods used to investigate the fracture evolution in folding processes. This research considered particles as a unit of matter (a rock block) to overcome scale-related methodological problems highlighted by previously published literature. The pre-existing fractures and the stress state in the model can simulate the geological history of anticline formation.

Calibration and characterization is essential to realibly reproduce the physical behavior of anticlines. Different contact model parameters imply different behavior and consequently different fracture evolution. If experimental macroproperty characterization of the rock is not possible, identification of the range of physically permissible values is of fundamental importance to characterize the rock used in simulations. Pre-modelling analysis is an important tool that avoid mechanical instability in the DEM. It provides a better understanding of the main folding mechanism through simplified models which allow us to define boundary conditions. Through dimensionless plots and analytical expressions, it is possible to take into account pre-buckled folds. The buckled anticline geometries must be such that the axial stress range of buckling, before the global shear failure is reached, is large enough to represent the natural folding evolution and ensuing fractures. Models of layer-parallel shortening should use these results. Pre-modelling analysis results can design models where the influence of burial depth is taken into account for shallow and deeper anticlines.

An extended domain of pre-buckled anticline must be modeled in layer-parallel shortening simulations. This model allows us to overcome the rigid wall boundary conditions influences and limitations. The addition of a breakable domain allows the natural anticline fracture evolution. Multi-layer results show the strong influence of the surrounding fractures on a single layer. Bending simulation results of a single layer and multi-layers provide a different fracture evolution. The loading process and the boundary conditions used strongly affect the fracture network and evolution. There is a need to further studies to understand how different interlayer properties, orientation and spacing of pre-existing fractures influence the following fracture mechanisms.

In conclusion, the discrete element method is a robust technique for forward and reverse simulations. If the strain rate of tectonic movement and natural boundary conditions are known, important insights concerning fracture network features can be inferred. Conversely, if the fracture network related to a single process is known, the stress and boundary conditions features can be deduced.

## APPENDIX – ROCKS EXPERIMENTAL DATA

Site	Sample description	$\sigma_3$ [MPa]	$\sigma_1$ [MPa]	$m_i$	$r$
Rapsomati	<b><i>Mitric Limestones</i></b>	0	60	22.1	0.96
		0	40		
		5	90		
		5	82		
		10	129		
		10	107		
		20	180		
		20	159		
Pelasgia	<b><i>Recrystallized micro-sparitic Limestones</i></b>	0	152	13.2	0.93
		0	125		
		0	208		
		12	242		
		12	170		
		12	254		
		24	291		
		24	299		
		36	321		
		36	352		
		48	382		
		48	429		

## REFERENCES

---

- Allwardt, P. F., Bellahsen, N., and Pollard, D. D. (2007). "Curvature and fracturing based on global positioning system data collected at Sheep Mountain anticline, Wyoming." *Geosphere*, 3(6), 408-421.
- Barton, N., and Choubey, V. (1977). "The shear strength of rock joints in theory and practice." *Rock Mechanics and Rock Engineering*, 10(1), 1-54.
- Bazalgette, L., and Petit, J.-P. (2007). "Fold amplification and style transition involving fractured dip-domain boundaries: buckling experiments in brittle paraffin wax multilayers and comparison with natural examples." *Geological Society, London, Special Publications*, 270(1), 157-169.
- Bergbauer, S., and Pollard, D. D. (2004). "A new conceptual fold-fracture model including prefolding joints, based on the Emigrant Gap anticline, Wyoming." *Geological Society of America Bulletin*, 116(3-4), 294-307.
- Boutt, D. F., and McPherson, B. J. (2002). "Simulation of sedimentary rock deformation: Lab-scale model calibration and parameterization." *Geophysical research letters*, 29(4).
- Burg, J. P. (2017). "Structural Geology and Tectonics: folding."
- Burg, J. P. (2017). "Structural Geology and Tectonics: Joints."
- Chen, P.-y. "Effects of Microparameters on Macroparameters of Flat-Jointed Bonded-Particle Materials and Suggestions on Trial-and-Error Method." *Geotechnical and Geological Engineering*, 1-15.
- Cooke, M. L., Simo, J., Underwood, C. A., and Rijken, P. (2006). "Mechanical stratigraphic controls on fracture patterns within carbonates and implications for groundwater flow." *Sedimentary Geology*, 184(3), 225-239.
- Corbett, K., Friedman, M., and Spang, J. (1987). "Fracture development and mechanical stratigraphy of Austin Chalk, Texas." *AAPG Bulletin*, 71(1), 17-28.
- Couples, G. D., Lewis, H., and Tanner, P. G. (1998). "Strain partitioning during flexural-slip folding." *Geological Society, London, Special Publications*, 127(1), 149-165.
- Cundall, P. A. "A computer model for simulating progressive, large-scale movements in blocky rock system." *Proc., Proc. Int. Symp. for ISRM, Nancy, Paper*.
- Cundall, P. A., and Hart, R. D. (1992). "Numerical modelling of discontinua." *Engineering computations*, 9(2), 101-113.
- Cundall, P. A., and Strack, O. D. (1979). "A discrete numerical model for granular assemblies." *geotechnique*, 29(1), 47-65.
- Di Naccio, D., Boncio, P., Cirilli, S., Casaglia, F., Morettini, E., Lavecchia, G., and Brozzetti, F. (2005). "Role of mechanical stratigraphy on fracture development in carbonate reservoirs: Insights from outcropping shallow water carbonates in the Umbria–Marche Apennines, Italy." *Journal of Volcanology and Geothermal Research*, 148(1), 98-115.
- Dolson, J. (2016). *Understanding oil and gas shows and seals in the search for hydrocarbons*, Springer.
- Donath, F. A., and Parker, R. B. (1964). "Folds and folding." *Geological Society of America Bulletin*, 75(1), 45-62.

- Donzé, F., Mora, P., and Magnier, S.-A. (1994). "Numerical simulation of faults and shear zones." *Geophysical Journal International*, 116(1), 46-52.
- Drummond, J. M. (1964). "An appraisal of fracture porosity." *Bulletin of Canadian Petroleum Geology*, 12(2), 226-245.
- Erickson, S. G. (1996). "Influence of mechanical stratigraphy on folding vs faulting." *Journal of Structural Geology*, 18(4), 443-450.
- Ericsson, J., McKean, H., and Hooper, R. (1998). "Facies and curvature controlled 3D fracture models in a Cretaceous carbonate reservoir, Arabian Gulf." *Geological Society, London, Special Publications*, 147(1), 299-312.
- Fakhimi, A., and Villegas, T. (2007). "Application of dimensional analysis in calibration of a discrete element model for rock deformation and fracture." *Rock Mechanics and Rock Engineering*, 40(2), 193-211.
- Ferrill, D., Morris, A., and Smart, K. (2007). "Stratigraphic control on extensional fault propagation folding: Big Brushy Canyon monocline, Sierra del Carmen, Texas." *Geological Society, London, Special Publications*, 292(1), 203-217.
- Fischer, M. P., and Wilkerson, M. S. (2000). "Predicting the orientation of joints from fold shape: Results of pseudo-three-dimensional modeling and curvature analysis." *Geology*, 28(1), 15-18.
- Galuppo, C., Toscani, G., Turrini, C., Bonini, L., and Seno, S. (2016). "Fracture patterns evolution in sandbox fault-related anticlines." *Italian Journal of Geosciences*, 135(1), 5-16.
- Gholipour, A. M. (1998). "Patterns and structural positions of productive fractures in the Asmari Reservoirs, Southwest Iran." *Journal of Canadian Petroleum Technology*, 37(01).
- Gross, M. R., Fischer, M. P., Engelder, T., and Greenfield, R. J. (1995). "Factors controlling joint spacing in interbedded sedimentary rocks: integrating numerical models with field observations from the Monterey Formation, USA." *Geological Society, London, Special Publications*, 92(1), 215-233.
- Guo, L., Latham, J.-P., and Xiang, J. (2017). "A numerical study of fracture spacing and through-going fracture formation in layered rocks." *International Journal of Solids and Structures*, 110, 44-57.
- Hayes, M., and Hanks, C. L. (2008). "Evolving mechanical stratigraphy during detachment folding." *Journal of Structural Geology*, 30(5), 548-564.
- Hennings, P. H., Olson, J. E., and Thompson, L. B. (2000). "Combining outcrop data and three-dimensional structural models to characterize fractured reservoirs: An example from Wyoming." *AAPG bulletin*, 84(6), 830-849.
- Howard, W. (1928). "A Classification of Limestone Reservoirs." *AAPG Bulletin*, 12(12), 1153-1161.
- Hubbert, M., and Willis, D. (1955). "Important fractured reservoirs in the United States." *45th World Pet. Cong. Proc., Section I/A-1*, 58-81.
- Itasca, U. (2011). "UDEC—Universal Distinct Element Code." *Itasca Consulting Group Inc., Minneapolis*.
- Ivars, D. M., Pierce, M. E., Darcel, C., Reyes-Montes, J., Potyondy, D. O., Young, R. P., and Cundall, P. A. (2011). "The synthetic rock mass approach for jointed rock mass modelling." *International Journal of Rock Mechanics and Mining Sciences*, 48(2), 219-244.

- Jaeger, J. C., Cook, N. G., and Zimmerman, R. (2009). *Fundamentals of rock mechanics*, John Wiley & Sons.
- Ji, S., ZHU, Z., and WANG, Z. (1998). "Relationship between joint spacing and bed thickness in sedimentary rocks: Effects of interbed slip." *Geological Magazine*, 135(05), 637-655.
- Keating, D. P., and Fischer, M. P. (2008). "An experimental evaluation of the curvature-strain relation in fault-related folds." *AAPG bulletin*, 92(7), 869-884.
- Laubach, S. E., Olson, J. E., and Gross, M. R. (2009). "Mechanical and fracture stratigraphy." *AAPG bulletin*, 93(11), 1413-1426.
- Lavrov, A. (2016). *Lost circulation: mechanisms and solutions*, Gulf Professional Publishing.
- Lisjak, A., and Grasselli, G. (2014). "A review of discrete modeling techniques for fracturing processes in discontinuous rock masses." *Journal of Rock Mechanics and Geotechnical Engineering*, 6(4), 301-314.
- Lucia, F. J. (2007). *Carbonate reservoir characterization: an integrated approach*, Springer Science & Business Media.
- Mas Ivars, D., Potyondy, D. O., Pierce, M., and Cundall, P. A. (2008). "The smooth-joint contact model." *Proceedings of WCCM8-ECCOMAS*, 2008, 8th.
- Masaferro, J. L., Bulnes, M., Poblet, J., and Casson, N. (2003). "Kinematic evolution and fracture prediction of the Valle Morado structure inferred from 3-D seismic data, Salta province, northwest Argentina." *AAPG bulletin*, 87(7), 1083-1104.
- McLeish, A. (1992). *Geological science*, Nelson Thornes.
- Mitra, S. (1990). "Fault-propagation folds: geometry, kinematic evolution, and hydrocarbon Traps (1)." *AAPG Bulletin*, 74(6), 921-945.
- Mitra, S. (2003). "A unified kinematic model for the evolution of detachment folds." *Journal of Structural Geology*, 25(10), 1659-1673.
- Mogi, K. (2007). *Experimental rock mechanics*, CRC Press.
- Muir, J. M. (1934). "Limestone reservoir rocks in the mexican oil fields." *Problems of Petroleum Geology. (Sydney Powers Memorial Volume): Tulsa, American Association of Petroleum Geologists*, 377-398.
- Murray Jr, G. H. (1968). "Quantitative Fracture Study--Sanish Pool, Mckenzie County, North Dakota." *AAPG Bulletin*, 52(1), 57-65.
- Narr, W., and Suppe, J. (1991). "Joint spacing in sedimentary rocks." *Journal of Structural Geology*, 13(9), 1037-1048.
- Nelson, R. (2001). *Geologic analysis of naturally fractured reservoirs*, Gulf Professional Publishing.
- O'Sullivan, C. (2011). *Particulate discrete element modelling*, Taylor & Francis.
- Patel, M. B., and Shah, M. "Strength Characteristics for Limestone and Dolomite Rock Matrix using Tri-Axial System."
- Paterson, M. S., and Wong, T.-f. (2005). *Experimental rock deformation-the brittle field*, Springer Science & Business Media.
- Potyondy, D. "A flat-jointed bonded-particle material for hard rock." *Proc., 46th US Rock mechanics/geomechanics symposium*, American Rock Mechanics Association.
- Potyondy, D. (2013). "PFC3D flat joint contact model version 1. Itasca Consulting Group." Minneapolis, Technical Memorandum ICG7234-L.

- Potyondy, D., and Cundall, P. (2004). "A bonded-particle model for rock." *International journal of rock mechanics and mining sciences*, 41(8), 1329-1364.
- Potyondy, D. O. (2015). "The bonded-particle model as a tool for rock mechanics research and application: current trends and future directions." *Geosystem Engineering*, 18(1), 1-28.
- Questiaux, J. M., Couples, G. D., and Ruby, N. (2010). "Fractured reservoirs with fracture corridors." *Geophysical Prospecting*, 58(2), 279-295.
- Ragan, D. M. (2009). *Structural geology: an introduction to geometrical techniques*, Cambridge University Press.
- Ramsay, J. G. (1967). *Folding and fracturing of rocks*, McGraw-Hill Companies.
- Ramsay, J. G., and Huber, M. I. (1987). *The techniques of modern structural geology*, Academic press.
- Rives, T., Razack, M., Petit, J.-P., and Rawnsley, K. (1992). "Joint spacing: analogue and numerical simulations." *Journal of Structural Geology*, 14(8-9), 925-937.
- Sabatoukakis, N., Koukis, G., Tsiambaos, G., and Papanakli, S. (2008). "Index properties and strength variation controlled by microstructure for sedimentary rocks." *Engineering Geology*, 97(1), 80-90.
- Saner, S., Al-Hinai, K., and Perincek, D. (2005). "Surface expressions of the Ghawar structure, Saudi Arabia." *Marine and petroleum geology*, 22(5), 657-670.
- Sanz, P. F., Pollard, D. D., Allwardt, P. F., and Borja, R. I. (2008). "Mechanical models of fracture reactivation and slip on bedding surfaces during folding of the asymmetric anticline at Sheep Mountain, Wyoming." *Journal of Structural Geology*, 30(9), 1177-1191.
- Smart, K. J., Ferrill, D. A., and Morris, A. P. (2009). "Impact of interlayer slip on fracture prediction from geomechanical models of fault-related folds." *AAPG bulletin*, 93(11), 1447-1458.
- Staff, A. (1959). "Ghawar Oil Field, Saudi Arabia." *Bulletin of the AAPG*, 43(2), 434-454.
- Starfield, A. M., and Cundall, P. "Towards a methodology for rock mechanics modelling." *Proc., International Journal of Rock Mechanics and Mining Sciences & Geomechanics Abstracts*, Elsevier, 99-106.
- Stearns, D. W., and Friedman, M. (1972). "Reservoirs in fractured rock: Geologic exploration methods."
- Stewart, S., and Podolski, R. (1998). "Curvature analysis of gridded geological surfaces." *Geological Society, London, Special Publications*, 127(1), 133-147.
- Suppe, J. (1983). "Geometry and kinematics of fault-bend folding." *American Journal of science*, 283(7), 684-721.
- Tsiambaos, G., and Sabatoukakis, N. (2004). "Considerations on strength of intact sedimentary rocks." *Engineering Geology*, 72(3), 261-273.
- Twiss, R. J., and Moores, E. (1992). "Structural Geology, 532 pp." WH Freeman, New York.
- Wang, Y., and Tonon, F. (2010). "Calibration of a discrete element model for intact rock up to its peak strength." *International journal for numerical and analytical methods in geomechanics*, 34(5), 447-469.
- Weatherley, D. (2009). "ESyS-Particle v2. 0 user's guide."

- Wennberg, O., Svåná, T., Azizzadeh, M., Aqrawi, A., Brockbank, P., Lyslo, K., and Ogilvie, S. (2006). "Fracture intensity vs. mechanical stratigraphy in platform top carbonates: the Aquitanian of the Asmari Formation, Khaviz Anticline, Zagros, SW Iran." *Petroleum Geoscience*, 12(3), 235-246.
- Winsberg, E. (2010). *Science in the age of computer simulation*, University of Chicago Press.
- Wu, S., and Xu, X. (2016). "A study of three intrinsic problems of the classic discrete element method using flat-joint model." *Rock Mechanics and Rock Engineering*, 49(5), 1813-1830.
- Yang, B., Jiao, Y., and Lei, S. (2006). "A study on the effects of microparameters on macroproperties for specimens created by bonded particles." *Engineering Computations*, 23(6), 607-631.